Convective Contribution to the Genesis of Hurricane Ophelia (2005)

Robert A. Houze Jr.

University of Washington, Seattle, Washington

Wen-Chau Lee and Michael M. Bell

National Center for Atmospheric Research, Boulder, Colorado

ABSTRACT

The convection occurring in the tropical depression that became Hurricane Ophelia (2005) was investigated just prior to tropical storm formation. Doppler radar showed a deep, wide, intense convective cell of a type that has been previously thought to occur in intensifying tropical depressions but has not heretofore been documented in detail. The updraft of the cell was 10 km wide, 17 km deep, had updrafts of 10–20 m s^{-1} throughout its mid- to upper levels, and contained a cyclonic vorticity maximum. The massive convective updraft was maintained by strong positive buoyancy, which was maximum at about the 10-km level, probably aided by latent heat of freezing. Evaporative cooling and precipitation drag occurred in the rain shower of the cell but were insufficient to produce a strong downdraft or gust front outflow to force the updraft. The convective updraft was fed by a layer of strong inflow that was several kilometers deep. Wind-induced turbulence, just above the ocean surface, enriched the equivalent potential temperature of the boundary layer of the inflow air, thus creating an unstable layer with little convective inhibition. This air was raised to its level of free convection when it encountered the denser air in the rainy core of the convection. The updraft motion and latent heat release in the intense cell generated potential vorticity throughout the low to midlevels, and contained a cyclonic vortex at the midlevels. Vorticity generated throughout the depth of the low to midtroposphere within convective updraft cells was subsequently incorporated into a stratiform region attached to the region of active convective cells. The vorticity perturbations at the low to midlevels in convective cells and their attached stratiform regions were available to be axisymmetrized into the larger-scale intensifying depression vortex.

1. Introduction

The genesis of tropical cyclones involves the concentration of perturbation kinetic energy onto the scale of a low pressure system with a horizontal scale of a few hundred kilometers. The concentration of energy on this scale is partly a downscale process, as a developing storm extracts energy from larger scales of motion. Gray (1968), DeMaria et al. (2001), Bracken and Bosart (2000), and McTaggart-Cowan et al. (2008) have examined the large-scale conditions favoring the genesis of Atlantic hurricanes. The latter study shows that in the Atlantic basin midlatitude and/or tropical synoptic-scale disturbances can set the stage for tropical cyclo-

genesis, with about half of the cases being of purely tropical background.

Tropical cyclogenesis also involves upscale processes, with convective-scale dynamics adding energy and vorticity to a preexisting cyclonic disturbance of the large-scale flow, possibly brought on by one of the larger-scale processes described by McTaggart-Cowan et al. (2008). These upscale processes are the topic of this paper. Studying western Atlantic tropical cyclones, Steranka et al. (1986) noted from satellite data that prolonged "convective bursts" occurred "in the near region surrounding the depression centers before the maximum winds initially increased." In this paper, we present and analyze a detailed set of observations in the convective burst region of a depression immediately before it intensified to tropical storm status and eventually became Hurricane Ophelia (2005).

The cloud cover analyzed in satellite photos by Steranka et al. (1986) is a gross indicator of a complex of convective entities that may populate a developing depression.

Corresponding author address: Robert A. Houze, Jr., Department of Atmospheric Sciences, University of Washington, Seattle, WA 98195.
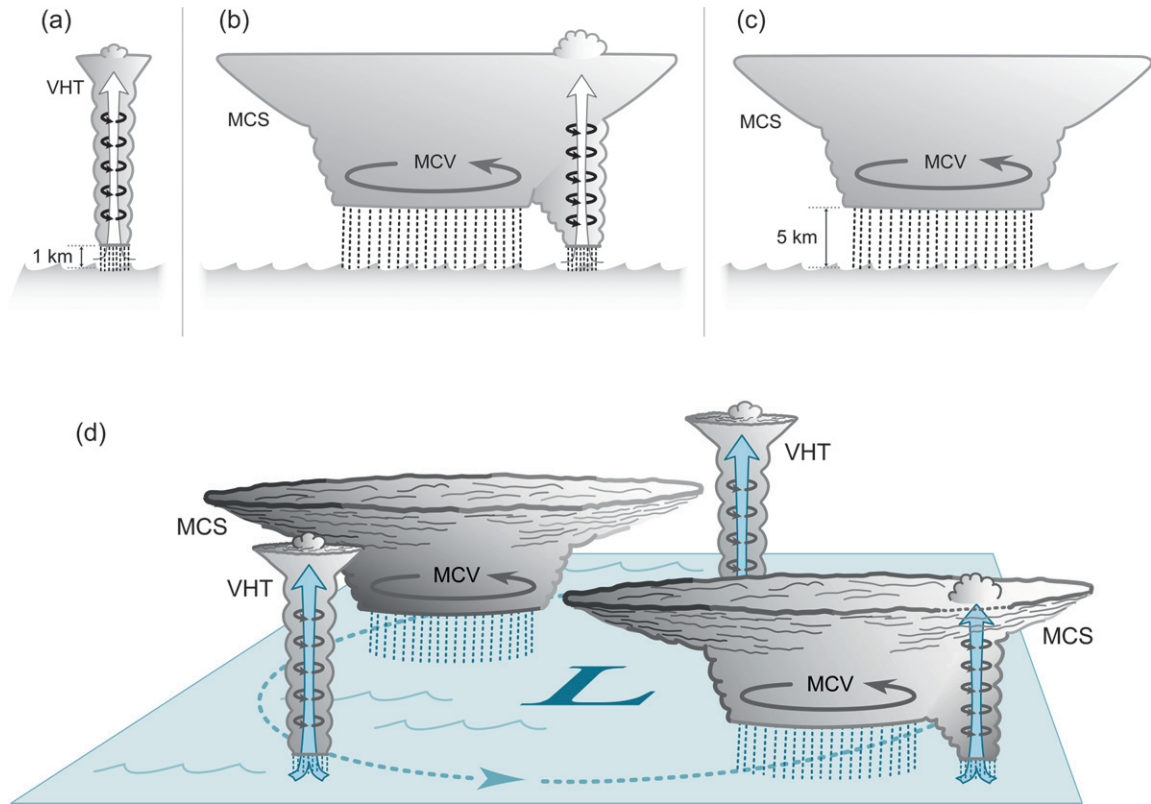E-mail: houze@washington.edu

FIG. 1. MCS life cycle within a developing tropical cyclone. (a) The MCS begins as a set of one or more isolated deep VHTs. The vorticity of the low-level environment is stretched by convergence in the lower portions of the updraft and advected upward. (b) The convective-scale cells are transient components of a larger and longer-lived MCS, and as individual VHTs of the MCS die off, they form a precipitating stratiform cloud out of the weakly buoyant upper portions of the old deep cells while new towers form, so that at its mature stage of development the MCS has both convective and stratiform components. The stratiform region accumulates the PV of the remaining portions of the convective cells to form a midlevel MCV. (c) In the late stages of the MCS life cycle, new cell development ceases, while the MCV vorticity remains in the precipitating stratiform cloud region for some hours. (d) An idealized distribution of VHTs and MCSs in various stages of development. The MCS life cyle is adapted from Houze (1982).

Figure 1 illustrates conceptually the variety of convective entities that may exist there. Some of these are individual convective towers, while others are mesoscale convective systems (MCSs), several hundred kilometers in horizontal dimension (see Houze 2004 for a review of MCSs). It has been suggested by Hendricks et al. (2004) and Montgomery et al. (2006) that the deep convective updrafts of these clouds are rotating, and they have called them vortical hot towers (VHTs) as a special case of the ''hot tower'' terminology introduced by Riehl and Malkus (1958) to describe deep tropical convection.[1]

---

[1] The term ''hot tower'' has also been used to describe tall, vertical, buoyant, rotating elements that are sometimes embedded in the eyewall of a fully developed hurricane (e.g., Heymsfield et al. 2001). Our use of the term refers to convection that occurs before the intensifying depression takes on the circulation characteristics of a tropical storm or hurricane.

Reasor et al. (2005) used Doppler radar data to indicate that that VHTs were present in the genesis phase of Hurricane Dolly (1996), and Sippel et al. (2006) found evidence of VHTs during the development of Tropical Storm Allison (2001). Our paper presents more detailed observational documentation of vortical convective updrafts in a depression actively intensifying into a tropical storm.

When several deep convective towers form in succession and near proximity they evolve into an MCS (Figs. 1a–c). A distinctive property of MCSs is that they develop regions of stratiform cloud and precipitation, composed of older convection (Houze 1997). The stratiform region tends to develop a mesoscale convective vortex (MCV) in midlevels (Fritsch et al. 1994). As suggested by Fig. 1, the clouds in a developing tropical cyclone consist of a population of individual convective towers and MCSs. Two types of hypotheses have been

proffered regarding how the population of convective towers and/or MCSs may constitute an upscale enhancement of tropical cyclogenesis.

The first type of upscale hypothesis involves MCVs located in the stratiform regions of MCSs. Ritchie and Holland (1997), Simpson et al. (1997), and Ritchie et al. (2003) hypothesized that a tropical cyclone forms when one or more MCSs revolve about the depression center (as in Fig. 1d) and reinforce the larger-scale depression. According to this hypothesis, each MCS spins up its own MCV in the stratiform region at midlevels, and this midlevel circulation feeds into the larger-scale depression circulation. This idea has been referred to as a "top-down" cyclogenesis mechanism because it explains how vorticity accumulates at midlevels, but the intensified depression vortex at midlevels would have to then build downward via an increasing Rossby penetration depth, advective processes, or some other mechanism to form a strong low-level incipient tropical cyclone. Bister and Emanuel (1997) suggested that cooling due to melting and evaporation of precipitation below the base of the stratiform cloud is involved in the extension of the midlevel MCV downward. However, the downdraft motions in the MCSs involved in tropical cyclogenesis do not appear to be very strong. Zipser and Gautier (1978) investigated the convection in an intensifying tropical depression and found little evidence of strong downdraft motion reaching the boundary layer as is common in ordinary MCSs such as squall lines (Zipser 1977). In the present paper, we also present evidence that downdrafts are of relatively minor importance in an MCS located in an intensifying tropical depression. In this paper, we suggest that the stratiform region may indeed be involved in aiding cyclogenesis at midlevels, but that at low levels the main players in the cyclogenesis are the deep convective-scale air motions.

The second type of upscale hypothesis for tropical cyclogenesis focuses on the active, buoyant convective cells of the MCSs that occur in a depression about to undergo transformation to a tropical storm. Nolan (2007) has presented idealized model results indicating that the moistening of the environment by the repeated occurrence of convective cells in a developing depression facilitates the conversion of the vortex to a tropical cyclone. Hendricks et al. (2004) and Montgomery et al. (2006) have suggested via modeling studies that the updrafts of deep convection in the vorticity-rich environment of a preexisting depression can develop vertical vorticity anomalies collocated with the updraft (i.e., vortical hot towers). They suggest that the VHTs are the building blocks of the tropical cyclone vortex that grows out of the pre-existing depression. Until now, the "bottom-up" mechanism has been examined primarily in the context

of models. Aircraft missions into developing Hurricane Dolly (1996) led Reasor et al. (2005) to advocate a stochastic view of tropical cyclone genesis in which the interplay of multiple low–midtropospheric MCVs and deep convective bursts initiate the surface circulation, but observational evidence that the convective cells in a developing tropical depression actually have a vortical nature has not been provided. In this paper, we present evidence that the deep convective cells in an intensifying depression have vortical updrafts, and we show how these updrafts may intensify the depression's vorticity at low levels.

This paper thus aims to advance the understanding of the upscale aspects of tropical cyclogenesis via observations and to determine the relative roles of the stratiform and convective elements of the MCSs in the upscale process. From a unique set of aircraft observations obtained in the Hurricane Rainband and Intensity Change Experiment (RAINEX; Houze et al. 2006, 2007), we will show how convection was operating in the tropical depression that turned into Hurricane Ophelia (2005). We will (i) show the detailed air motion structure within one of the several MCSs present in the depression, and (ii) examine both the convective and stratiform components of the MCS to understand how the MCS as a unit was contributing to the cyclogenesis. While we will present evidence that corroborates the basic notion of a vortical hot tower route to cyclogenesis, we will also suggest that it is simplistic to think only of the convective cells in this process. The convective cells tend to operate in the context of an MCS, and the stratiform region of the MCS also appears to play a role, though it is a role made possible by the convective-scale drafts from which the stratiform region is formed, and it is not a role in which significant downdrafts are important.

The study of Zipser and Gautier (1978) foreshadowed the present paper. They found that an MCS located in an intensifying tropical depression off the coast of Africa, in a zone of frequent cyclogenesis (McTaggart-Cowan et al. 2008), differed strikingly from ordinary MCSs in that it was dominated by a giant $\sim$15-km-wide updraft of $\sim$10 m s^{-1} at a flight level of 6 km (460 hPa), and downdrafts were of only minor importance in the boundary layer. They found that the MCS accounted for the majority of upward mass flux in the depression and that the low-level convergence supporting the MCS could stretch the environmental vorticity at a rate that would account for much of the intensification of the parent depression. This prior study of Zipser and Gautier suggests that the RAINEX results presented below have a generality beyond an individual case study. Our results obtained during the genesis of Ophelia both confirm their earlier findings and (with the aid of modern
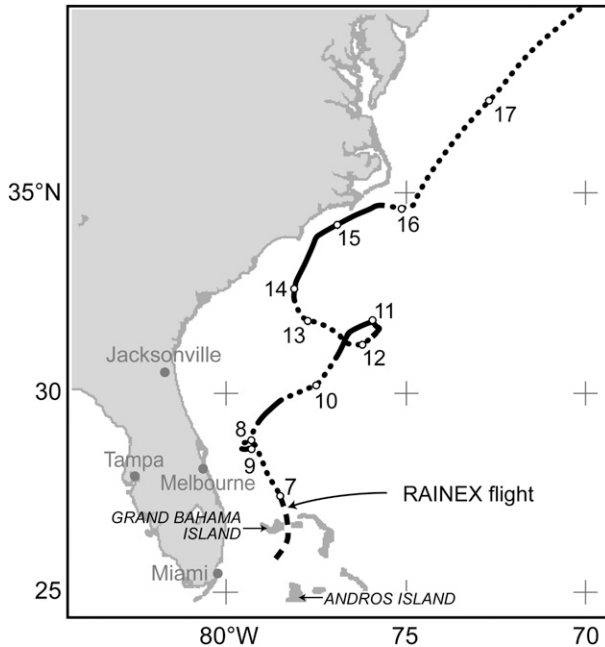
FIG. 2. Track of Hurricane Ophelia (2005): Depression stage (dashed), tropical storm stage (dotted), and hurricane stage (solid).

FIG. 3. Pressure and maximum wind throughout the lifetime of Ophelia.

aircraft Doppler radar data) extend their results to indicate *how* this peculiar form of convection operating in an intensifying depression contributes to the upscale development of the tropical cyclone.

2. Ophelia's history and development stage

Figure 2 shows the track of Ophelia, which began as a depression in the Bahamas, just north of Andros Island. The aircraft mission described in this paper took place on 6 September 2005, when the depression was just north of Grand Bahama Island. Figure 3 shows that the mission occurred immediately prior to when the depression began its intensification to tropical storm, and ultimately hurricane, status.

Figure 4 shows the synoptic-scale context of the genesis of Ophelia. On 6–7 September 2005, the 500-hPa map showed a broad ridge extending over the eastern United States, with almost no pressure gradient whatsoever. At 1200 UTC 6 September (Fig. 4a), one contour enclosed a weak low just off the southeast coast of Florida, at the location of the depression that would become Ophelia. By 0000 UTC 7 September (Fig. 4b), the depression had turned into Tropical Storm Ophelia, and the 500-hPa analysis showed a closed contour of positive vorticity that grew a bit larger by 1200 UTC (Fig. 4c).

Figure 5 shows infrared satellite and coastal radar imagery of the genesis stage of Ophelia. The cloud patterns in the infrared images correspond to the prolonged
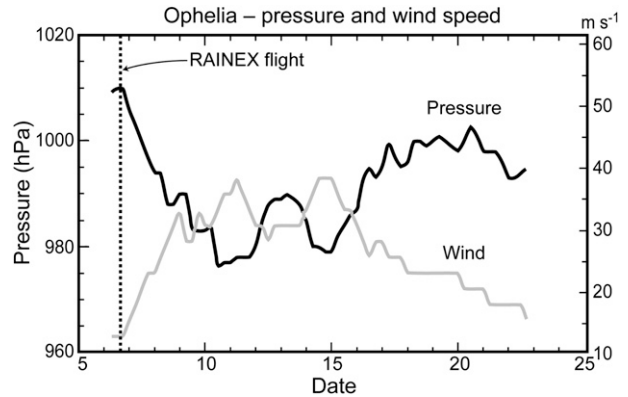
convective burst identified by Steranka et al. (1986). The cloud and precipitation entities in the infrared images and radar data in Fig. 5 are similar to those seen by Simpson et al. (1997) and Ritchie et al. (2003), who describe the cloud features as MCSs orbiting around the center of the developing Southern Hemisphere Tropical Storm Oliver (1993). The data in Fig. 5 are also similar to satellite and ground-based radar observations described by Sippel et al. (2006) of the newly formed Tropical Storm Allison (2001) making landfall in Texas. Sippel et al. (2006) further noted that the convective cells of the MCSs had positive vorticity anomalies shown by the single-Doppler ground-based radar data, indicating the presence of VHTs in the MCSs present during this cyclogenesis event. The Ophelia dataset described in this paper shows further details of VHTs in a similar tropical cyclogenesis situation.

Figures 5a,b show the cloud and precipitation pattern about 6 h prior to the aircraft mission described in this paper. The infrared satellite data in Fig. 5a show that convection was prevalent over a wide area just off the southeast coast of the United States. Tropical Storm Ophelia eventually formed in this area of enhanced high cloudiness. The cloudy area and storm genesis were close enough to the coast to be in view of the Melbourne, FL, Weather Surveillance Radar-1988 Doppler (WSR-88D) radar. Figure 5b shows the Melbourne radar reflectivity pattern corresponding to the satellite data in Fig. 5b (a time-lapse loop of the radar images can be obtained online from ftp://ftp.atmos.washington.edu/houze/OpheliaMovie). The convection located mostly to the east of Melbourne was producing heavy precipitation in a pattern that had no suggestion of tropical storm structure. Convective cells indicated by high reflectivity cores occurred throughout the region. The cells tended to be clustered in groups, and areas of less intense, stratiform precipitation were attached to some

of these groups of convection. The sizes of the stratiform regions were ~100–200 km in horizontal dimension, and they likely formed from the weakening of the convective cells (Houze 1997). Figures 5c,d are for the time of the aircraft mission described in this paper. The radar data for this time shows that the convection had grouped into three MCSs ~200 km in horizontal dimension, each having both active convective cells and areas of stratiform precipitation.[2] The aircraft mission investigated the middle of these three large systems. After the time of the aircraft mission, the convection continued to occur in mesoscale systems; however, by the time of Figs. 5e,f the overall area covered by deep convection decreased and became focused on a single mesoscale precipitation area to the east-northeast of Melbourne. In the next half-day, this mesoscale precipitation area radically changed its shape and took on the structure of a tropical storm (Figs. 5g,h). Nolan's (2007) idealized model results suggest that the long period of moistening by prior convection (e.g., Figs. 5a–d) may have facilitated this ultimate conversion from MCS to tropical storm structure. This radar echo exhibited an incipient eyewall and a principal rainband (as defined by Willoughby et al. 1984; Willoughby 1988) extending from south to east to north of the storm and having a convective structure upwind and a stratiform structure downwind, as described in papers on mature hurricane rainbands (Atlas et al. 1963; Barnes et al. 1983; Hence and Houze 2008). Time-lapse viewing of the radar data shows that the new principal rainband grew by systematically forming new convection on its upwind end. Smaller rainbands located both east and west of the new storm center were propagating radially outward.

3. The aircraft mission

The RAINEX aircraft mission on 6 September 2005 was conducted by a Naval Research Laboratory (NRL)

P3 aircraft flying in coordination with a National Oceanic and Atmospheric Administration (NOAA) P3 aircraft (Houze et al. 2006). The aircraft data obtained in the middle mesoscale system shown in Fig. 5d provide insight into the type of convection that leads to tropical cyclogenesis. Every year, the Hurricane Research Division (HRD) of NOAA carries out research flights into tropical cyclones as part of their Hurricane Field Program. An extensive and detailed flight plan is published prior to each year's program (the HRD Field Program Plans for the last 10 yr are available online at www.aoml.noaa.gov/hrd/). For many years HRD has maintained a convective burst flight pattern in their field program plan. However, it has seldom been executed because it is extremely difficult to catch tropical cyclogenesis in progress. In 2005, the convective burst flight track was executed in the genesis phase of Tropical Storm Gert (Halverson et al. 2007) and in the depression phase of Hurricane Ophelia. The study presented here is an analysis of the dataset collected in the Ophelia convective burst flight.

Since the genesis of Ophelia took place just off the coast of Florida on 7 September 2005, and a RAINEX multiaircraft mission had been planned for the later hours of 6 September, the opportunity arose to execute the HRD convective burst pattern at a key time in the history of the storm. This fortuitous circumstance was further advantaged by the availability of the ELDORA radar on the NRL P3 aircraft used in RAINEX (Houze et al. 2006, 2007). The Electra Doppler Radar (ELDORA) provided an especially high-resolution view of the details of convective burst phenomenon. The characteristics of ELDORA are described by Hildebrand et al. (1996). The radar has a wavelength of 3.2 cm, a peak transmitted power of 32 kW, and a beam width of 1.8° with 150-m gate spacing. It operates with two beams, pointing ~16.5° fore and aft, that overlap as the NRL P3 flies by convection with ~400-m sampling distance.

Figure 6 shows the generic HRD flight plan for a convective burst, as it appeared in HRD's Hurricane Field Program Plan. The essential component is a Doppler radar aircraft circumnavigation of the MCS comprising the convective burst. The second part of the track is a follow-on fly-by of the most intense convective element. In the case described here, the Doppler radar aircraft was the NRL P3 with ELDORA on board. As will be shown, both the circumnavigation and the close-up fly-by of the intense convective element were executed by the ELDORA aircraft.

The ability to successfully execute the convective burst flight plan in real time was facilitated by the fact that RAINEX aircraft missions were directed from a RAINEX Operations Center (ROC) on the ground (for details see Houze et al. 2006). All the participating
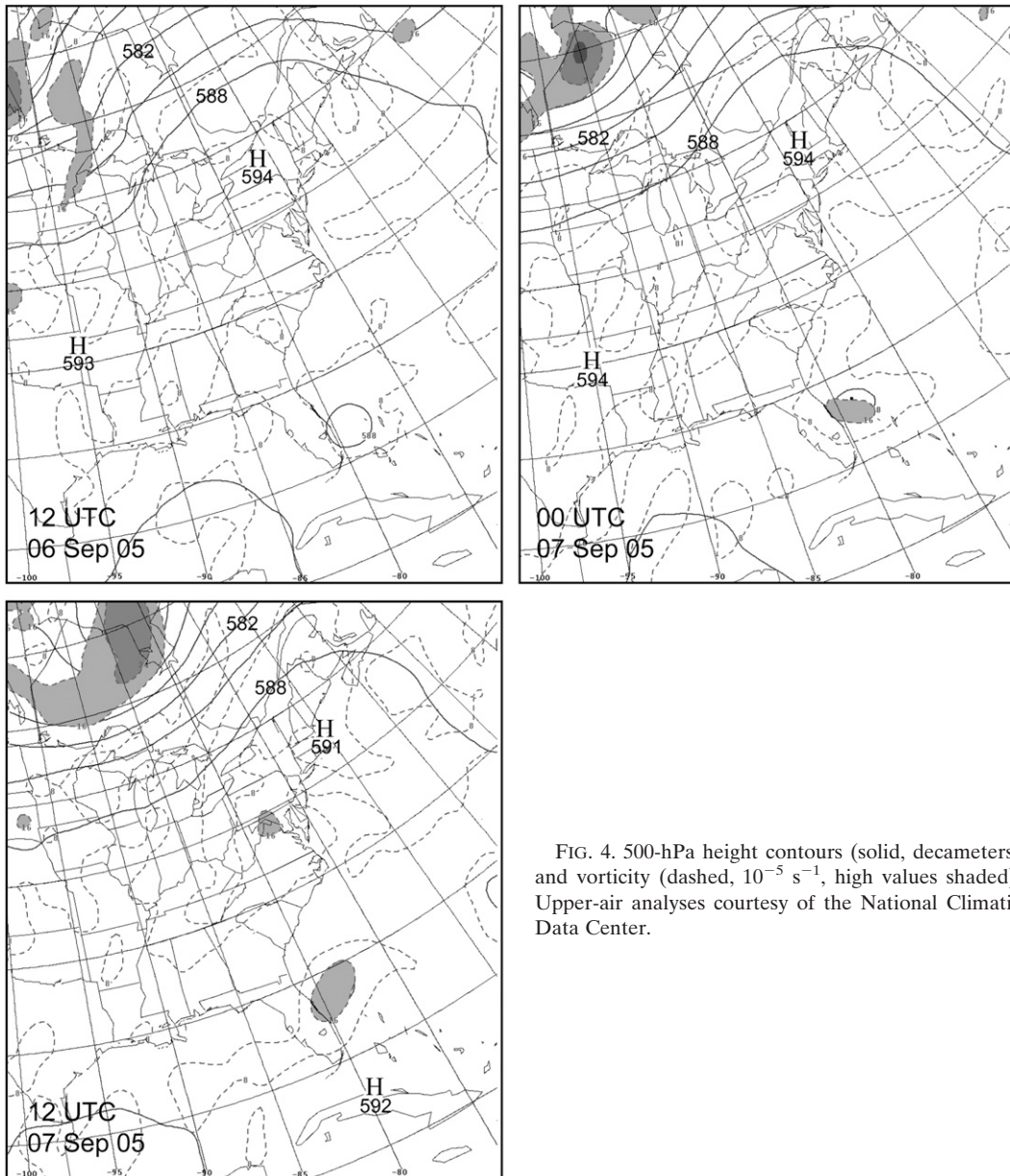
---

[2] Reviewing the loop of Melbourne radar data reveals that for many hours the depression was populated by rain areas ~100–200 km in dimension. Rain areas of this size are MCSs (as defined by Houze 2004 and others). They were made up partially of intense rain cells and partially of lighter rain (probably weakened cells that had turned stratiform). It is difficult to define the lifetimes of the individual MCS entities because they are continually merging and splitting. But each MCS seems to maintain an individual identity for a few hours. The aggregate of splitting and merging MCSs continues for tens of hours, probably because the intensifying depression was providing a favorable environment for the formation of new convection throughout the time period. Whether spreading cold pools were involved in the merging and splitting is not possible to determine definitively from any available dataset. However, structurally speaking, the patterns of radar echo evolving over the time period of the loop do not exhibit arc lines that would be indicative of gust front initiation of convective cells.

FIG. 4. 500-hPa height contours (solid, decameters) and vorticity (dashed, 10^{-5} s^{-1}, high values shaded). Upper-air analyses courtesy of the National Climatic Data Center.

aircraft were in contact with the ROC via Internet chat using air-to-ground satellite links. The NOAA P3 aircraft provided broad surveillance based on its lower-fuselage 5.5-cm wavelength scanning radar (Aberson et al. 2006). Surveillance radar data being obtained by NOAA P3 aircraft were transmitted by satellite link to the ROC every 5 min. The positions of both aircraft were also transmitted to the ROC, where a continually updated composite map based on the NOAA P3 surveillance radar, combined with satellite imagery, data from coastal radar data, and flight tracks of the aircraft was constructed. This real-time composite map of the mission was based on the radar data transmitted from the aircraft to

the ROC every 5 min. The lead author working in the ROC (on the ground) with this composite map communicated with the coauthors working aboard the NRL P3 to direct the NRL P3 into a flight pattern corresponding to the schematic convective burst plan in Fig. 6. This real-time direction of the NRL P3 led to the collection of the ELDORA data described in this paper.

Figure 7 shows the actual flight track, superimposed on the radar echo from the Melbourne WSR-88D radar. The NRL P3 approached the MCS from the south-southeast. The circumnavigation began on the southeast corner of the convective region and proceeded first north-northwestward. The aircraft turned to the west
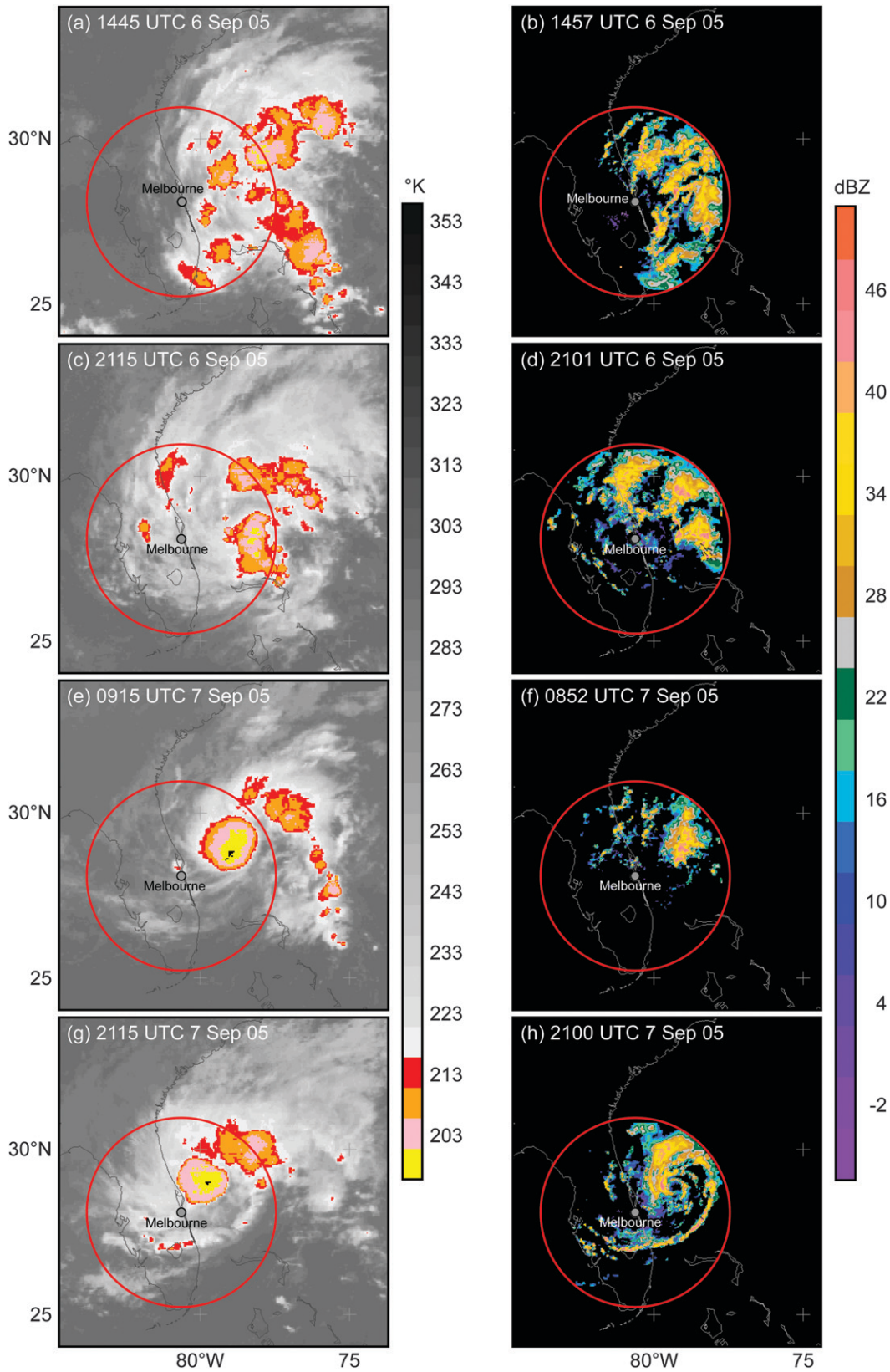
FIG. 5. Satellite and radar overview of the genesis of Ophelia. The circle shows the maximum radar range. Satellite imagery shows infrared temperature from *GOES-12*. Radar data are from the Melbourne, FL, WSR-88D.
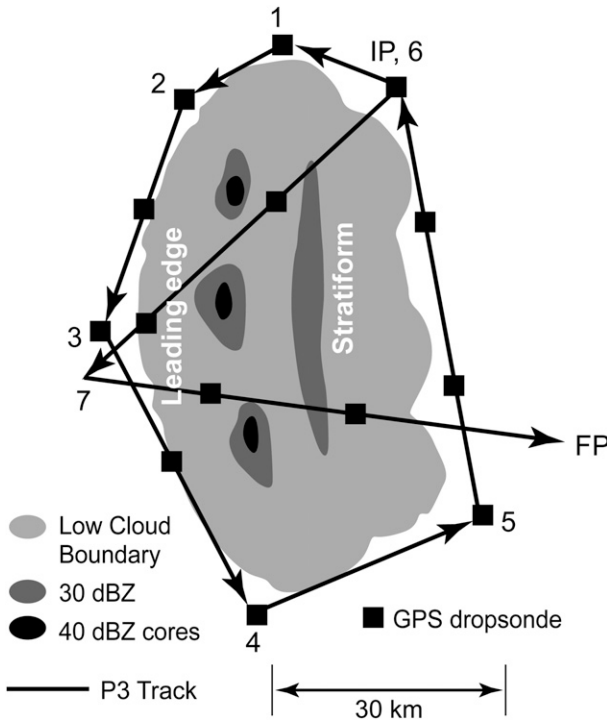
FIG. 6. Idealized flight plan for a ''convective burst'' as presented in the NOAA/HRD Hurricane Field Program Plan of 2005 and previous years. The arrows show the proposed track of a Doppler radar aircraft. The squares show the proposed dropsonde locations.
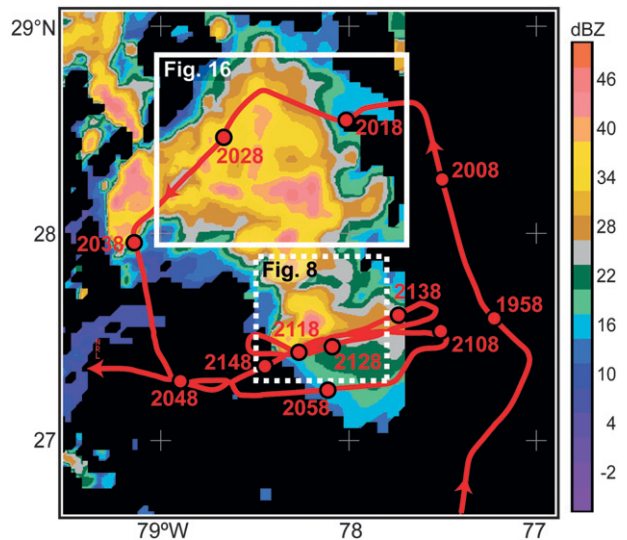

FIG. 7. Actual flight track (red) of the NRL P3 on 6 Sep 2005 in the depression that became Hurricane Ophelia. The times of the dropsondes are indicated. Radar data are from the Melbourne, FL, WSR-88D at 2101 UTC 6 Sep 2005. The boxes show the domains analyzed in Figs. 8 and 16.

and then to the southwest as it flew along the northern periphery of the stratiform portion of the MCS. Finally the aircraft turned east-northeastward from the southwest corner of the MCS and flew along the southern side of the MCS, along the southern edge of the region containing the strong convective cell to be described below. The aircraft then reversed course 3 times on the southern edge of the MCS to do successive close-up fly-bys of the most intense convective cell. The boxes in the figure show two regions that we focus on in the remainder of this paper, and the locations of dropsondes are indicated along the flight track.

4. The convective cell

a. Depth, width, and intensity of the updraft

Figures 8a,c show the convective radar echo detected by ELDORA on the three successive close-up fly-bys. Figure 8d is a vertical cross section taken along the red line in Fig. 8a at ~2113 UTC. The convective cell was extremely deep, reaching up to about 17 km in echo-top height. The 40-dBZ echo reached above 12 km, which is a rare event over tropical oceans in general and off the coast of Florida in particular (Zipser et al. 2006). The

echo core had dBZ values reaching the upper 40s at low levels, and it extended upward through a horizontally extensive anvil echo. Vectors of the air motion in the plane of the cross section in Fig. 8d further show that the region of updraft was very wide, with a horizontal scale of ~10 km at most levels in this cross section. With our analysis tools, we were able to view numerous cross sections through the convective region. The width varied somewhat from one section to another (only one such section is shown for illustration in Fig. 8) and with altitude, but was typically 10–15 km. The updraft observed in an intensifying tropical depression by Zipser and Gautier (1978) was of similar horizontal scale; the flight track across the cell in their case was ~20 km (see Fig. 14 of their paper). The updraft seen in Figs. 8c,d was also very intense. At 6 km the updrafts were ~10 m s^{-1} all across the 10-km-wide cell, almost exactly the intensity found by Zipser and Gautier (1978) all across the 15-km-wide cell at a flight level of 6 km. The ELDORA data are shown in a vertical cross section in Figs. 8d,e, where Fig. 8e zooms in on the middle portion of Fig. 8d. These panels show that at levels above 6 km, the vertical velocities were even greater, everywhere 10–20 m s^{-1} or more throughout the upper volume of the deep updraft.

b. No gust front—Possible wind-induced mixing

One of the striking aspects of the wide, deep, and intense convective cell seen in Fig. 8d is the near absence of a significant downdraft. Even in the heavy precipitation
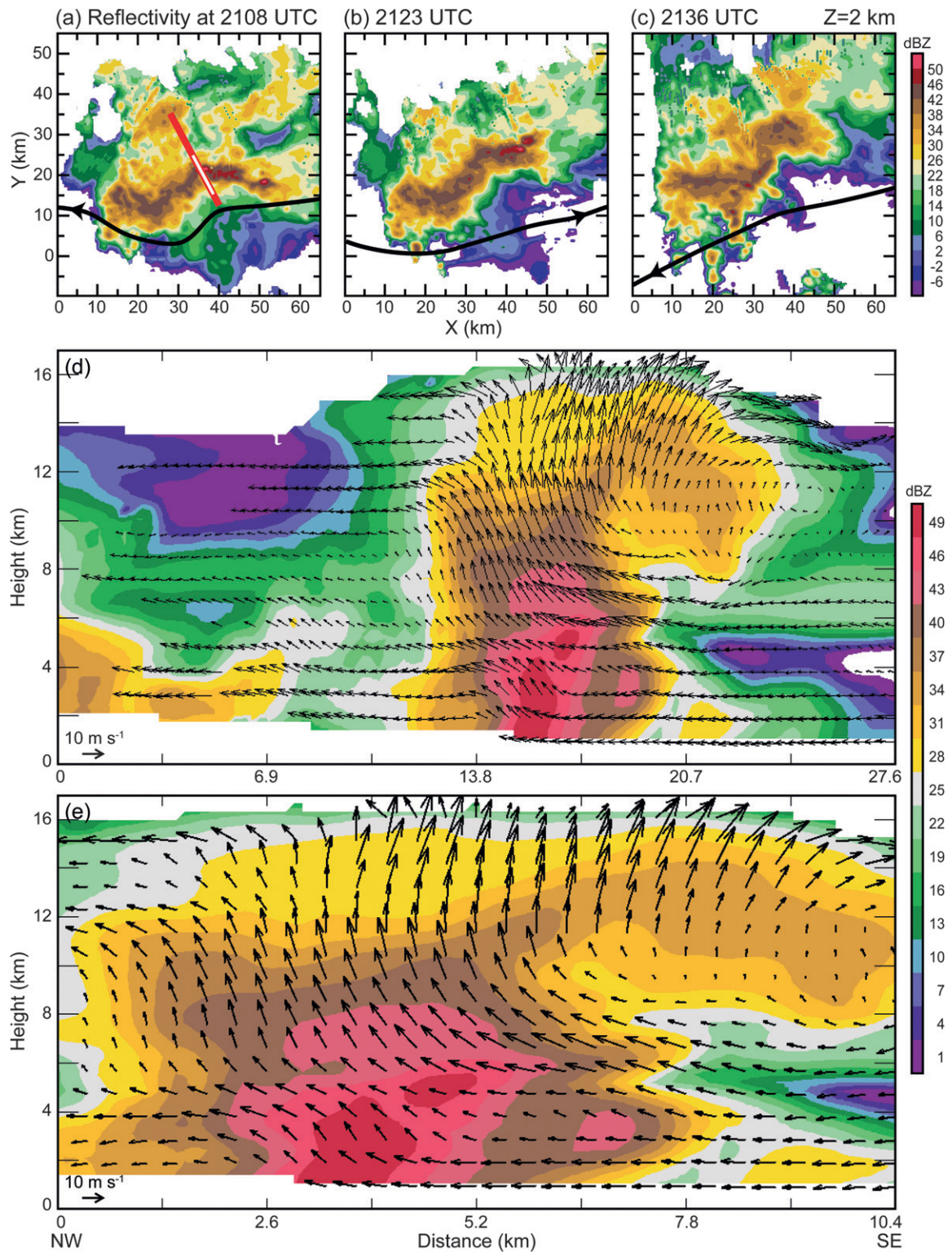
FIG. 8. (a)–(c) ELDORA radar reflectivity at the 2-km level for the three fly-bys of the intense convective cell. The times indicate the beginning of the 10–15-min passes by the convective feature. (d) Vertical cross section from northwest (NW) to southeast (SE) along the longer (red) line of (a). (e) Vertical cross section along the shorter (white) line of (a). Cartesian domains are relative to National Hurricane Center best-track position of Ophelia at 0000 UTC 7 Sep 2005.

core, where precipitation-driven downdrafts are found in ordinary cumulonimbus clouds (Zipser 1977), only updraft motion was evident. Absolutely no gust front convergence was evident. Instead the strong south-easterly airflow at the lowest levels, on the northeast side of the depression, flowed under the cell directly across the precipitation core of the cell. To see this aspect of the ELDORA winds more clearly, we have zoomed in on the region of the heavy precipitation core in Fig. 8e. Zipser and Gautier (1978) also found that the massive convective element they observed in an intensifying tropical depression was primarily an updraft. At the level of their boundary layer flight, about 150 m above the ocean, they noted that "there was no evidence of significant penetration of the subcloud layer by convective-scale downdrafts of lower than ambient equivalent potential temperature nor of any squall-like winds."

In general, tropical mesoscale convective systems exhibit deep wide updrafts paired with comparably robust downdraft outflows (e.g., Kingsmill and Houze 1999). Absent such gust front convergence to force parcels above their levels of free convection, the remarkable convective updraft, which penetrated to +17 km, must have become buoyant by some other mechanism. We note the strong horizontal flow at low levels approaching the storm and flowing directly under the cell in Fig. 8e. Boundary layer mixing enhanced by the strong low-level winds (Emanuel 1986, 1987; Yano and Emanuel 1991; Emanuel et al. 1994) would have increased the vapor content and equivalent potential temperature of the boundary layer so that parcels entering the base of the updraft would be extremely buoyant and the boundary layer lapse rate would be steep with little convective inhibition. Although the aircraft did not fly in the boundary layer, the dropsonde data obtained as the NRL P3 flew along the track shown in Fig. 7 are consistent with this reasoning. Figure 9 contains three soundings obtained just upwind of the giant convective cell. Each of these soundings shows strong southeasterly flow below the 800-hPa level. The thermodynamic profiles are a bit noisy, but each sounding clearly shows a very steep (nearly dry adiabatic) lapse rate just above the ocean surface (below about 950 hPa). Above 950 hPa, the temperature was close to a moist adiabat. Clearly buoyancy was available from the surface layer.

Xu and Emanuel (1989) pointed out that oceanic tropical soundings tend to be nearly moist adiabatic. The potential buoyancy of lifted parcels of air is indicated by the extent to which the surface and/or boundary layer–equivalent potential temperature exceeds that of the moist adiabat characterizing the free atmosphere. The nearly dry adiabatic lapse rate in the boundary layer
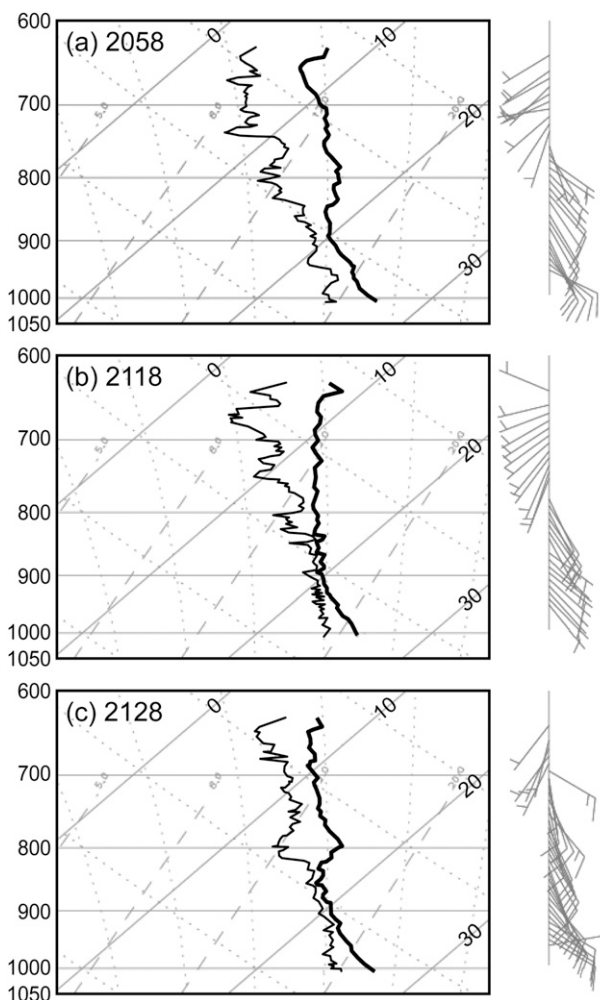

FIG. 9. Dropsonde data taken in the region of inflow to convective cell. The locations of soundings are in Fig. 7. Plots are in skew T–log p format. One wind barb = 10 m s^{-1}.

shown in Fig. 7 indicates that, if lifted slightly, the boundary layer air approaching the deep convective cell from the southwest with high equivalent potential temperature and little or no convective inhibition as a result of its apparent wind-induced mixing would become strongly buoyant.

The question is how the lifting to saturation would occur in the absence of a strong downdraft gust front. Some other mechanism must have triggered the initial lift of the parcel. Crook and Moncrieff (1988) showed in model calculations that the cooling at low levels produced by the evaporation of rain could produce a sufficient density gradient for the low-level airflow feeding the deep convection to converge and rise in the precipitation zone, without coming to rest at a stagnation point as it would if it were encountering a downdraft gust front. They called this mechanism a "gravity wave

without stagnation.'' The low-level flow seen in our Figs. 8d,e and 14a was similar to their idealized flow (cf. with their Fig. 15a). No stagnation point was reached, and air at the lowest levels flowed through the rain curtain, but rose as it encountered the rain area. Even though the rain shower did not produce a strong downdraft, the evaporation and weight of the raindrops were sufficient to produce a density gradient at low levels that composed an obstacle to the flow. The incoming air was then able to rise enough for parcels to travel above their level of free convection and realize the intense convection. In section 4e, we will show that the Doppler radar data are thermodynamically consistent with this idea.

According to Crook and Moncrieff (1988), this type of lifting in the rain shower zone is especially favored in a region characterized by general large-scale convergence, which lifts the low-level air toward saturation and thus decreases convective inhibition. The intensifying tropical depression, such as the one investigated by Zipser and Gautier (1978) and the case examined herein, is characterized by strong synoptic-scale convergence and is thus an ideal environment in which triggering of deep convection can occur without downdraft gust front triggering.

c. Deep inflow

Another notable feature of the convective cell evident in Figs. 8d,e is the depth of the layer of air feeding into the wide, intense updraft. The strong vertical velocities concentrated in the upper portion of the updraft constituted a strong vertical mass flux aloft, which had to be compensated by a deep layer of inflow. Kingsmill and Houze (1999) have shown that deep layers of inflow are common when convection takes on a mesoscale organization. The deep layer of inflow seen in this case, moreover, was likely potentially unstable and might have constituted a ''moist absolutely unstable layer'' (Bryan and Fritsch 2000; Mechem et al. 2002). In any case, the inflow to the deep, wide, intense cell observed by ELDORA was not composed simply of boundary layer air. In the cross section of Fig. 8e, the deep layer of inflow had two maxima: one below 4 km and the other at about 6 km (see right-hand boundary of the figure panel). The upper maximum may have been a response to the release of latent heat of freezing at the upper levels.

d. Evolution of the three-dimensional airflow

The detailed airflow pattern seen during the first fly-by, at 2108 UTC (Fig. 8a), is shown in Fig. 10. At 1.6 km, the flow was nearly uniformly flowing into the line of convection from the southeast (Fig. 10a). At 14 km,

the flow was diverging outward from the echo core (Fig. 10c). At 6 km, the flow had a more complex pattern (Fig. 10b), which is better understood in terms of the perturbation wind (defined by removing the mean wind over the entire echo in the domain of the figure panel). The perturbation wind shows a vortex couplet centered on the convective cell (Fig. 10d). A vortex couplet of this type would be expected as a linear consequence of the tilting of the environment shear by the updraft producing the cell (Rotunno 1981; Houze 1993, 292–295). The positive member of the vorticity couplet appears to be somewhat broader than the negative member, as might be expected since the convection was occurring in a vorticity-rich depression. The low-level convergence feeding the updraft would be expected to stretch this environmental vorticity, and the updraft would transport this locally intensified positive vorticity upward. Thus, the midlevels would be expected to contain positive vorticity both from the tilting of environment vorticity and from the stretching and upward advection of vorticity by the updraft.

Fifteen minutes later, at 2123 UTC, the second fly-by showed a similar uniform southeasterly inflow to the convective line at low levels (Fig. 11a), and the divergent outflow centered on the cell was stronger than at the previous time (Fig. 11c). The midlevel flow exhibited a single cyclonic vortex, seen at 6 km in both the total wind (Fig. 11b) and the perturbation wind (Fig. 11c). Figure 11d shows that this circulation was centered on the positive vorticity perturbation at 6 km. At this time the negative vorticity center just to the northwest of the positive vorticity center was relatively weak.

After 11 more minutes, at 2134 UTC, the third fly-by again showed uniform southeasterly inflow at 1.6 km (Fig. 12a) and divergent outflow at 14 km (Fig. 12c). The positive vorticity perturbation centered on the cell at 6 km was even stronger than it was during the previous fly-by.

e. Buoyancy and pressure perturbation

The data obtained by ELDORA on the fly-bys provided a full three-dimensional wind field at three separate times. Using this information it was possible to perform a thermodynamic retrieval, as described in the appendix. With the Doppler-derived wind field as input to the equation of motion and thermodynamic equation, the retrieval yields the pressure and temperature perturbation fields over the domain of radar observations. Anelastic mass continuity is used as a constraint and solutions are obtained by a variational technique that minimizes errors over the whole spatial domain. Time derivatives were determined by using the wind syntheses for the fly-bys at 2108 and 2123 UTC (Figs. 8a,b).
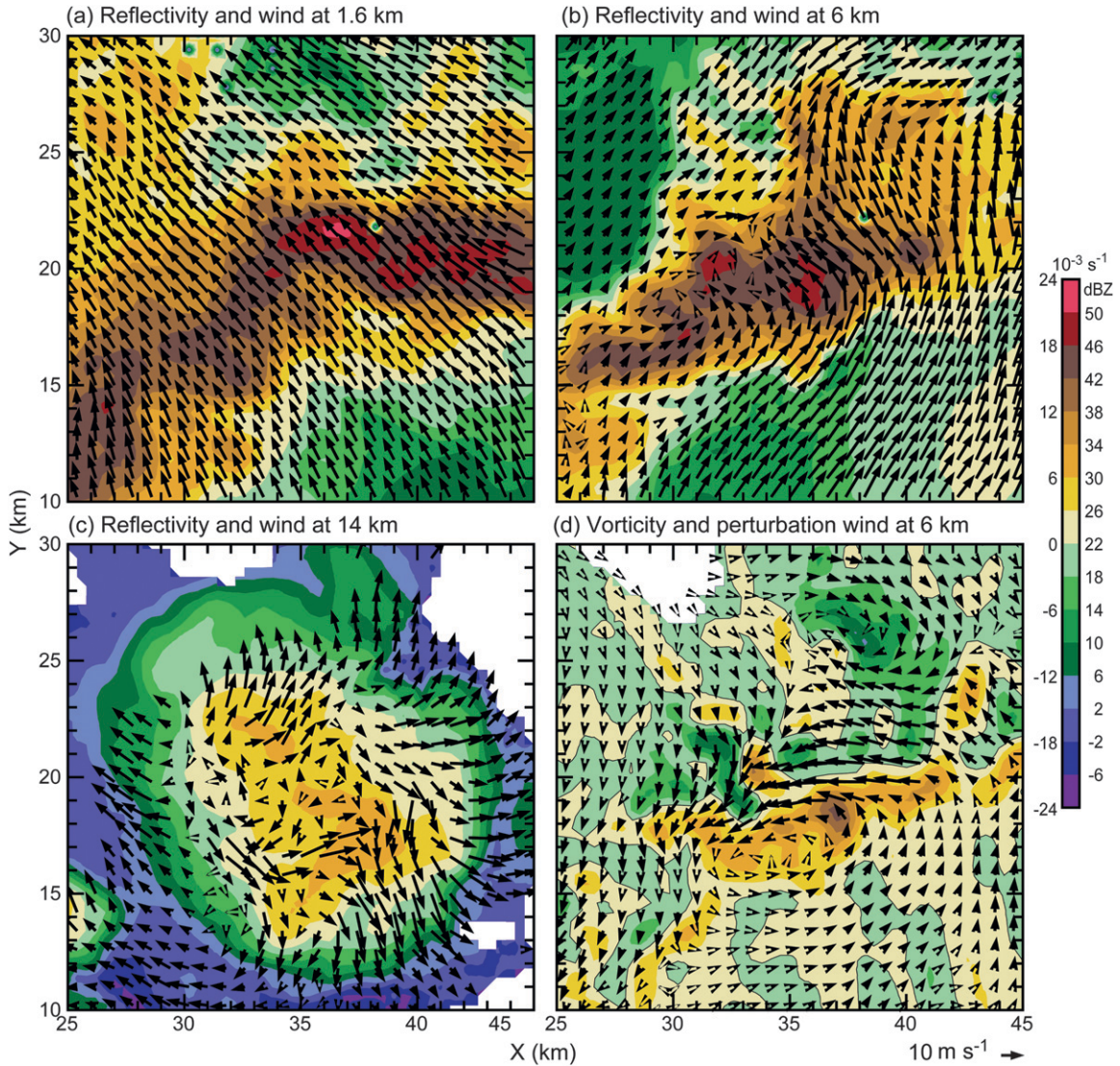
FIG. 10. Synthesis of wind fields from the ELDORA radar data obtained in a subregion of Fig. 8a at 2108–2122 UTC 5 Sep 2005. Reflectivity (color, dBZ) and ground relative wind vectors are shown at (a) 1.6-, (b) 6-, and (c) 14-km altitudes. (d) Relative vorticity (color, 10^{-3} s^{-1}) and perturbation wind vectors defined by removing the mean wind over the larger domain shown in Fig. 8 at each vertical level. Cartesian domain is relative to National Hurricane Center best-track position of Ophelia at 0000 UTC 7 Sep 2005.

Figure 13 shows results of the thermodynamic retrieval at the 8-km level. The plot is roughly centered on the updraft, which was ~10 km in horizontal dimension. The background color of the plot shows the vorticity, which was strongly positive (cyclonic) in the updraft region, and collocated with a positive temperature perturbation. Negative (anticyclonic) vorticity was found on the fringes of the updraft and was smaller in both magnitude and area covered than the cyclonic vorticity. The perturbation wind field took the form of a closed cyclonic vortex, indicating that the updraft was rotating. The pressure perturbation contours conformed to the perturbation wind field, indicating that the wind and pressure fields

had nearly adjusted to each other, thus implying that the energy of the rotational flow was to a large degree not propagating away from the convective region; that is, some rotation remained trapped in the cell. This negative pressure perturbation had a magnitude of 0.5 hPa and was slightly offset from the maximum temperature perturbation, which exceeded 4°C.

A vertical cross section through the updraft of the convective element at 2108 UTC reveals much about its structure and dynamics (Fig. 14a). This convective cell was extraordinarily deep and intense by any measure. The updraft reached 17 km in height. An echo of 30 dBZ was present all the way up to ~14 km, indicating
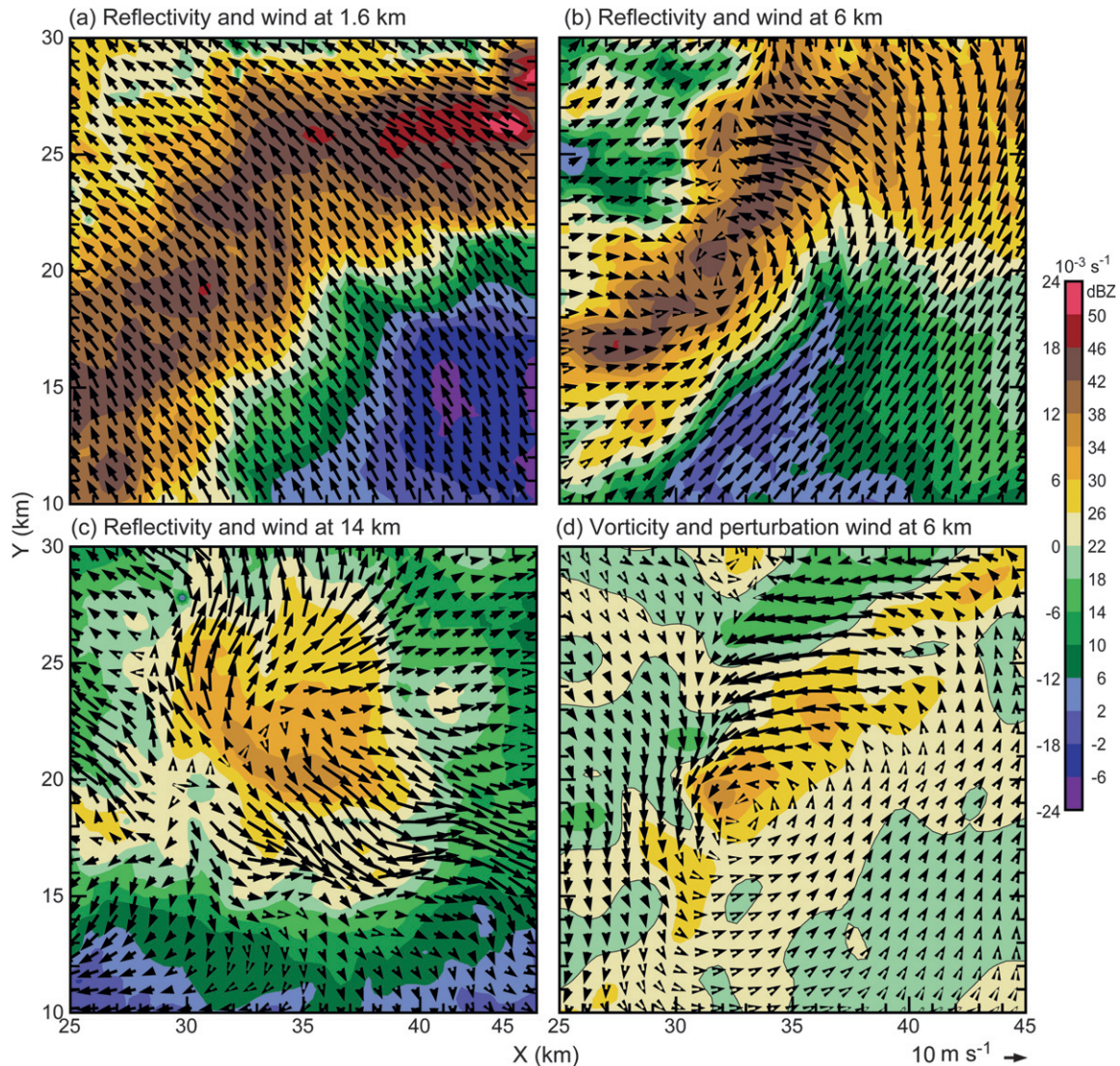
FIG. 11. As in Fig. 10, but for 2123–2135 UTC 5 Sep 2005.

the production of large graupel particles in the strong updraft. Above the 7-km level the updraft was $>10 \text{ m s}^{-1}$ in magnitude throughout the volume of the storm—over a region approximately 10 km wide and 10 km deep! At lower levels the updraft was less intense (although still several meters per second) but covered a wider area, approximately 15 km wide. The peak temperature perturbation (marked in the figure) was $>6°C$ at the 10-km level. The occurrence of the maximum buoyancy at this level suggests that latent heat of freezing was important in driving the cell to great heights. Zipser (2003, see his Fig. 5.4) points out that latent heat of freezing can provide a buoyant boost of ∼2°C between 6- and 14-km height. At low levels, below ∼3 km, the buoyancy perturbation was weakly negative ($<-1.5°C$

at its absolute minimum). This negative buoyancy was located at the base of the rain shower constituting the core of the cell. A pressure perturbation of about -0.5 hPa was located atop this cool layer at $X = 38$ km, $Z \approx 4$ km, just at the location where the low-level inflow air was turning upward. A second negative pressure perturbation of $\simeq 0.5$ hPa at $X = 38$ km, $Z \approx 7.5$ km. This upper pressure perturbation minimum was probably dynamically produced; it was located at the center of the circulation in the updraft seen in Fig. 13.

The negatively buoyant pool at the base of the rain cell was apparently strong enough to act as an impediment that turned the unstable inflow air upward so that it could become buoyant. However, this negative buoyancy was not strong enough to generate a downdraft and
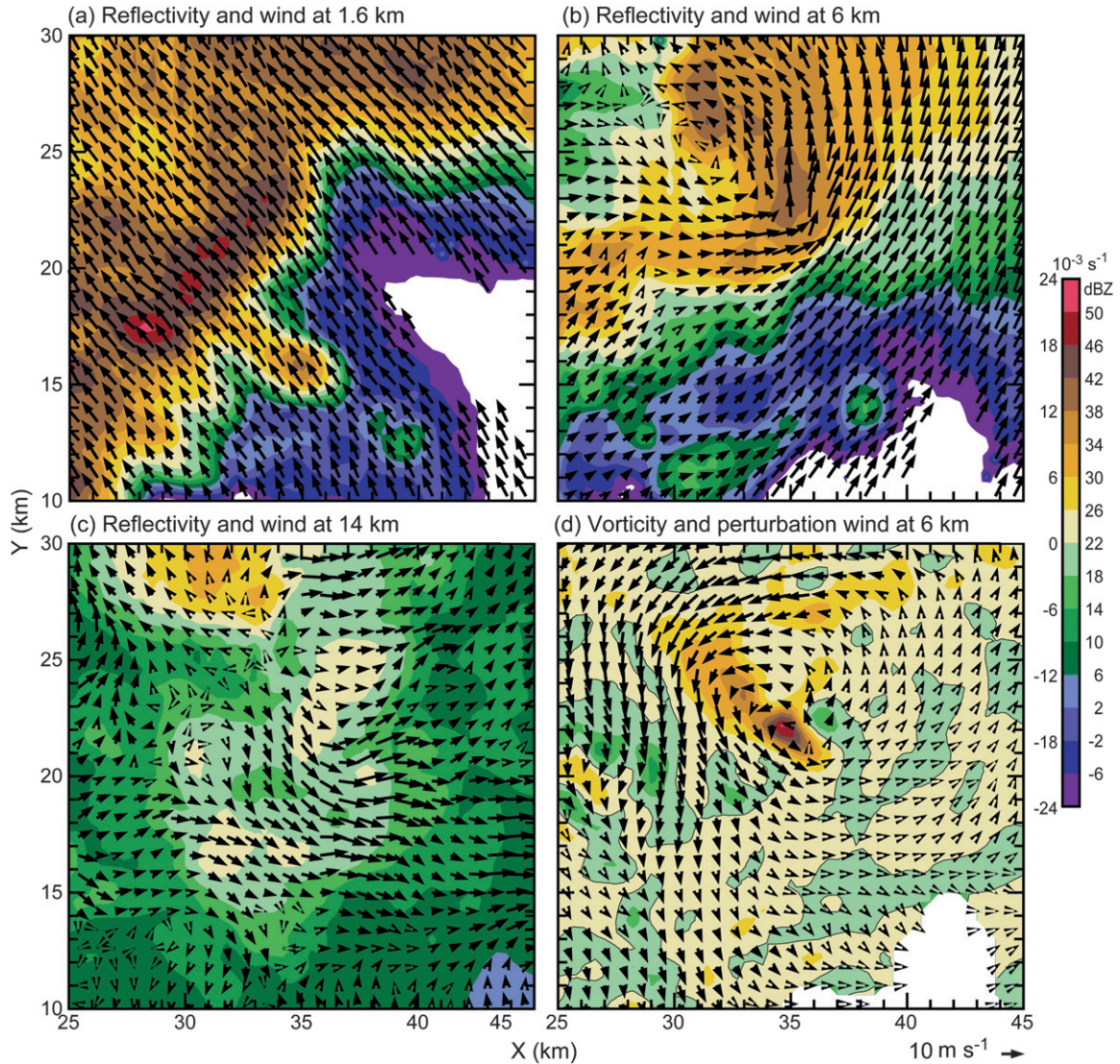
FIG. 12. As in Fig. 10, but for 2136–2150 UTC 5 Sep 2005.

density current outflow pool. As noted in section 4b, this observed structure is consistent with the modeling study of Crook and Moncrieff (1988).

Figure 14a shows that upper-level downdrafts were surrounding the top portion of the updraft in echo minimum zones just outside of and adjacent to the towers at levels above 9 km. These upper-level downdrafts were evidently forced by the perturbation pressure gradient field outside the buoyant towers in the manner discussed by Houze (1993, 223–226) and Yuter and Houze (1995a, see their appendix B).

f. Vertical mass flux and potential vorticity generation

The similarity of convection seen over the region of the depression (e.g., Figs. 5b,d) suggests that cells of the type illustrated in Fig. 14a collectively accounted for enormous mass transport in the mid- to upper troposphere throughout the region where tropical cyclogenesis was about to occur. In Fig. 14b, the color field displays vertical mass transport ρw. The maximum of vertical mass transport associated with the broad, deep, and intense updraft occupying the entire volume of the storm from the mid to upper levels is evident, with an absolute maximum at about the 9-km level. Since the vertical mass transport is proportional to latent heating, the vertical mass transport pattern implies a strong maximum of heating aloft.

Potential vorticity (PV) production is directly proportional to the vertical gradient of latent heating. As a proxy for PV production, we have plotted contours of
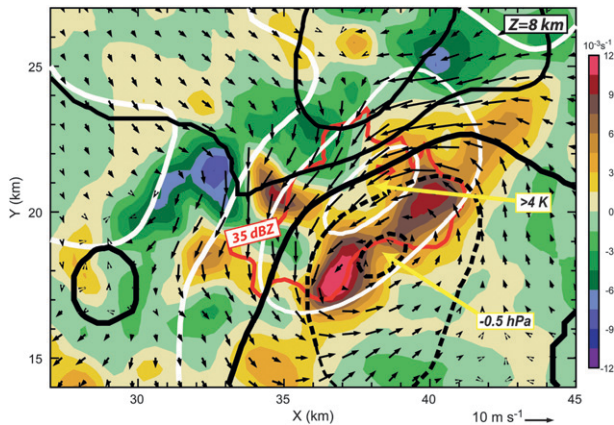
FIG. 13. Buoyancy retrieval from ELDORA based on ELDORA wind fields observed at 2108 and 2123 UTC shown in Figs. 8a,b. Results are shown for the 8-km level. Relative vertical vorticity (color, 10^{-3} s^{-1}) is shown with perturbation wind vectors, and overlaid with the buoyancy field in units of virtual potential temperature perturbation (θ_v', white lines, 1-K contours), perturbation pressure (black lines, 0.5-hPa contours). Thicker lines indicate zero contours, solid lines are positive, and dashed lines show negative perturbations. The red contour surrounds the region where reflectivity is >35 dBZ. Cartesian domain is relative to National Hurricane Center best-track position of Ophelia at 0000 UTC 7 Sep 2005.

$\partial(\rho w)/\partial z$ in Fig. 14b. These contours show that the cell was generating PV throughout the low to midtroposphere. To the extent that all the convection in the depression was acting in a way similar to this convective cell, the convective population (Figs. 5a–d) was contributing to a bottom-up form of tropical cyclogenesis (as discussed in section 1), culminating in the development of tropical storm Ophelia (Figs. 5g,h), and ultimately Hurricane Ophelia. To investigate how the vertical mass flux changed with time, we have computed statistics of the mass flux for each of the three fly-by times (Figs. 8a–c). The left-hand panels of Fig. 15 show the mean mass flux profiles for each time. The right-hand panels show the mass fluxes in contoured frequency by altitude diagrams (CFADs; Yuter and Houze 1995a,b). The CFADS show contours of the mass flux accounted for by different vertical velocities at each height in the storm. It should be noted that these statistics are for the entire volume of echo, not just the large convective cell dominating the picture in Fig. 14. In the large cell, downdraft activity was nearly absent. However, the statistics in Fig. 15 show that the region surrounding the cell contained downdrafts, although overall the updrafts dominated the net mass flux at all levels. Nolan's (2007) idealized model results also suggest that as the developing depression becomes humidified by convection, updrafts become deeper and stronger while downdraft frequency is unchanged.

The results for 2108 UTC in Figs. 15a,b are for the time illustrated by Figs. 13 and 14. In general the CFADs are similar to those for ordinary convection observed in non–tropical cyclone environments (cf. Fig. 3 of Yuter and Houze 1995b). The mass flux profile in Fig. 15a shows that the overall mass flux was greater at low levels at this time. Recall that in Fig. 14b, there were maxima of ρw and $\partial(\rho w)/\partial z$ throughout a wide area of the lower troposphere in a kind of skirt surrounding the intense deep updraft cell at this time. The positive vertical gradient of mass flux at the low levels was accounted for by the accumulated effect of the weaker updraft velocities—not by extreme values of vertical velocity. The CFAD in Fig. 15b shows that at the low levels the mass flux was dominated by weaker updrafts (<5 m s^{-1}). The bulk effect of the weaker convective updraft velocities thus accounted for the PV generation (contributing to cyclogenesis) at the lower levels.

The extreme vertical velocities in the giant cell seen in Figs. 8 and 14 were found at higher levels. The outer contour of the CFADs in Fig. 15 is the signature of these extreme updrafts at upper levels. The CFADs in Fig. 15 show, however, that the bulk of the mass transport at upper levels was also by weaker updrafts (<5 m s^{-1}). It is likely that these weaker updrafts were the remnants of extreme updrafts that had occurred earlier. At any given time the population of updrafts at upper levels likely consisted of a few extreme drafts such as those depicted in Figs. 8 and 14, but also many drafts that were previously strong but had dropped off in intensity. This wide range of core sizes and strengths contributing to the mass flux within regions of convection is rather typical (Yuter and Houze 1995b; May and Rajopadhyaya 1999). As time progressed, the overall mass transport at upper levels grew in strength (Figs. 15c–f), likely as more remnants of earlier intense updrafts accumulated aloft. The bimodal character of the mass flux at the later times may be a sampling variation, or possibly it could be related to the latent heat of fusion enhancing the updrafts at upper levels.

At all times in Fig. 15, there was a strong vertical gradient of mass flux at low levels, indicating that at each of the analysis times there was PV generation occurring at the low levels. This indicates that the bottom-up process of PV generation was active in this convective region at all times. As time went on, the maximum of mass transport became more elevated and the convective PV generation was occurring at a range of altitudes, from low to midlevels. Over time the vertical profile of vertical mass transport develops a double maximum. The upper maximum was likely related to the buoyancy boost at upper levels owing to release of latent heat of freezing. The horizontal inflow required by mass
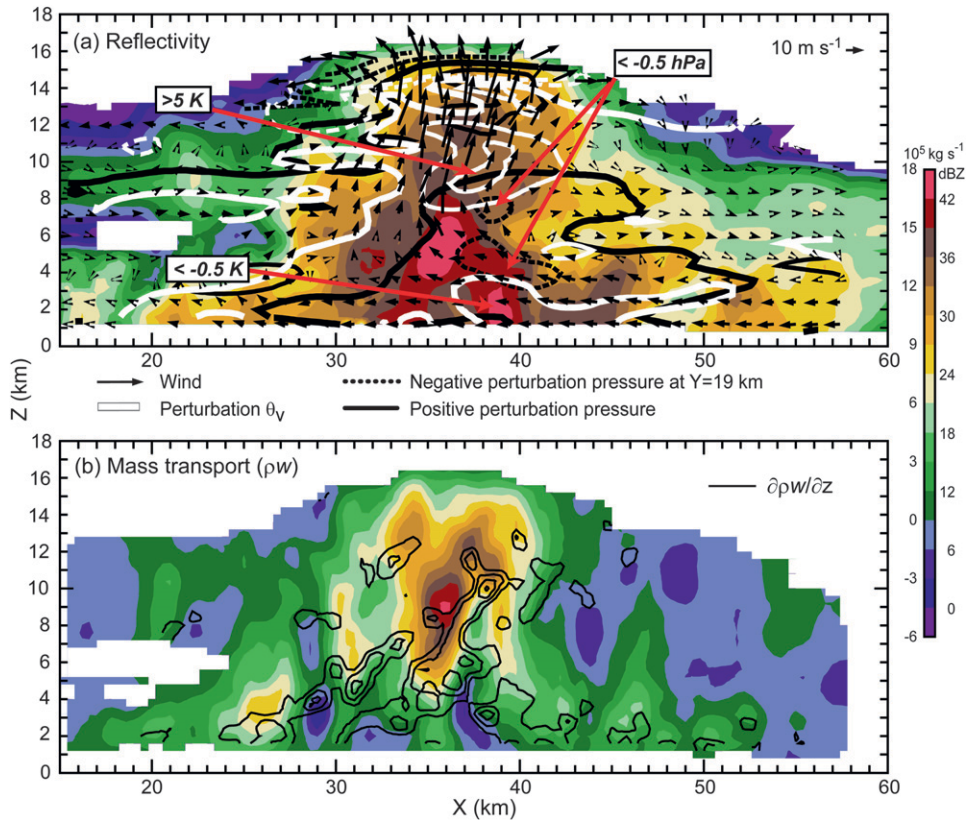
FIG. 14. Vertical slice through ELDORA radar analysis based on observation volumes obtained at 2108 and 2123 UTC 6 Sep 2005. Section is taken along $Y = 19$ km in Figs. 8a,b and 13. (a) Reflectivity (color, dBZ) with wind vectors, overlaid with the buoyancy field in units of virtual potential temperature perturbation (θ_v', white lines, 2.5-K contours) and perturbation pressure field (black lines, 0.5-hPa contours). Thicker lines indicate zero contours, solid lines are positive, and dashed lines are negative perturbations. Velocity vectors are in the X–Z plane. (b) Mass transport (color, 10^5 kg s^{-1}) and areas of positive vertical mass transport gradient (units = 2×10^5 kg s^{-1} m^{-1} with contours starting at 1×10^5 kg s^{-1} m^{-1}). Cartesian domain is relative to National Hurricane Center position of Ophelia at 0000 UTC 7 Sep 2005.

continuity correspondingly had two layers, as seen in Figs. 8d,e. The vertical gradient of heating associated with the double maximum implies that PV generation also had two maxima, one at the lower levels (below ~3 km) and another in the midlevels (~6–9 km), with the upper maxima developing in the later stages of the intense convective cell seen in Fig. 8.

5. Stratiform region characteristics

The convective element described in detail above was part of a mesoscale convective system (the middle system of Fig. 5d). Mesoscale convective systems typically consist of both active convective cells and an adjoining region of stratiform precipitation. ELDORA observed mostly stratiform radar echo on the northern portion of the flight track shown in Fig. 7. A dual-Doppler synthesis was performed for the region of the box surrounding that part of the flight track in Fig. 7. The radar echo detected

by ELDORA in this region is illustrated in Fig. 16. The flight track relative to the predominantly stratiform radar echo is shown in Fig. 16a. A vertical cross section through the reflectivity pattern is shown in Fig. 16b. The echo in this section is typical of the region. A bright band was evident, but the echo pattern also showed pockets of higher echo intensity with fall streaks sloping downward from maxima in the brightband reflectivity. This type of echo is indicative of stratiform precipitation forming from the weakening and dissolution of previously active convective cells (Fig. 6.11 of Houze 1993; Fig. 1 of Houze 1997; Fig. 4 of Yuter and Houze 1997).

Figure 17 shows the wind pattern at 6 km derived from ELDORA. The winds were flowing into the storm from the southeast at this level (Fig. 17a). The perturbation winds exhibited a general cyclonic circulation over the whole region and a cellular pattern of vorticity, in which numerous small-scale centers of positive vorticity outnumbered and outweighed small-scale centers of
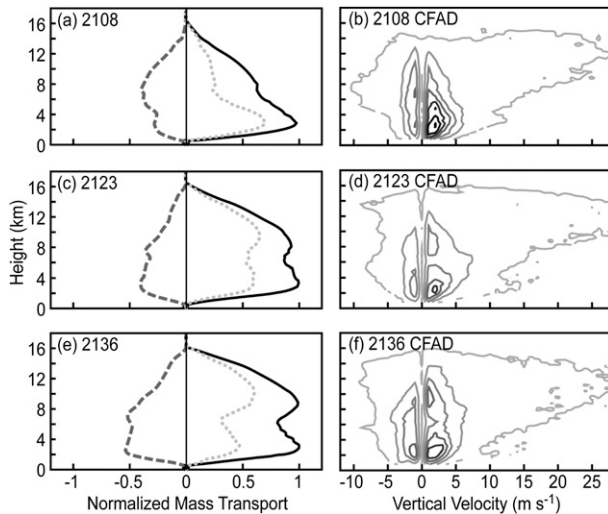
FIG. 15. Vertical mass transport in the convective. (left) Total mass transport normalized to the peak positive value for the three convective analysis times shown in Figs. 8a–c. Black lines indicate upward transport, dashed lines denote downward transport, and the dotted line is net transport. (right) Vertical-mass-transport-weighted CFADs of vertical velocity. The CFADs show the frequency of vertical velocities in a given range (w to $w + \Delta w$) occurring in a given height interval (z to $z + \Delta z$), with the frequency weighted by vertical mass transport ρw, where ρ is the air density. The contours indicate the amount of vertical mass transport accounted for by each combination w and z. The contour units are 10^6 kg s^{-1}, with the 30×10^6 kg s^{-1} contour highlighted. Data are binned in 1 m s^{-1} vertical velocity increments.
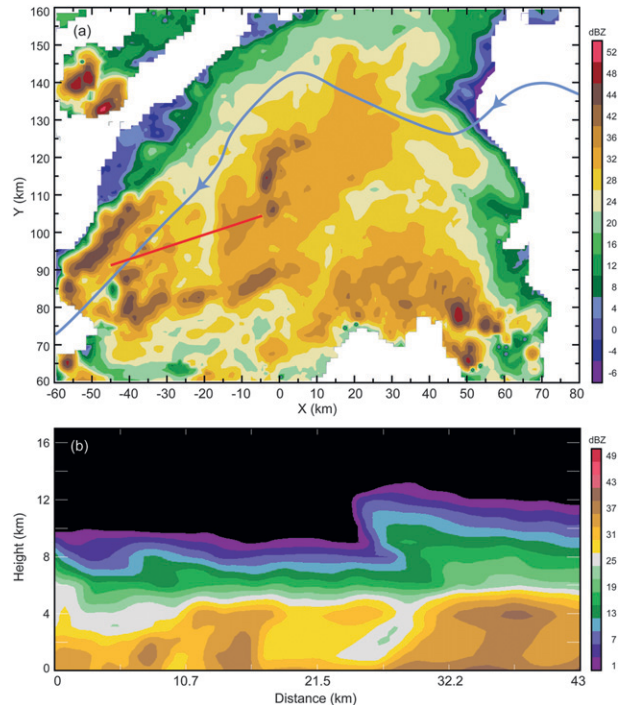

FIG. 16. (a) ELDORA flight track and radar reflectivity at 2-km altitude for the stratiform region observed at 2005–2040 UTC 6 Sep 2005. (b) Reflectivity cross section along the red line in (a). Cartesian domain is relative to 0000 UTC 7 Sep 2005 National Hurricane Center best-track position.

negative vorticity. Evidently, weakening and dissolving convective cells, over time, left a population of mostly positive small-scale vorticity perturbations in the mid- to upper levels as the old cells blended into the stratiform region of the mesoscale convective system. Figure 13 shows that the upper portion of the intense convective cell contained a cyclonic circulation ~10 km wide that approximately conformed to the pressure perturbation isobars, indicating that the updraft's upper region consisted of a quasi-balanced circulation. As noted in section 4e, this behavior would have trapped convective-scale vorticity within the cell. If all the convective cells blending into the stratiform region were of this type, each would have retained and contributed positive vorticity to the widening stratiform region. The net of this vorticity accumulated from these old cells apparently composed the cyclonic circulation seen in the perturbation winds in Fig. 17.

We further investigated the stratiform region shown in Fig. 17 by examining the mean vertical mass flux profile and a mass-flux-weighted CFAD based on the vertical air motions derived from the ELDORA data (Fig. 18). As expected for a stratiform region made up of dying convection, both updrafts and downdrafts

were observed. However, unlike the stratiform regions of ordinary mesoscale convective systems (e.g., Yuter and Houze 1995a,b), *net* downward motion did not occur in the mid- to low levels of the stratiform region. Updraft motions outweighed downdraft motions at the lower levels so that the net vertical air motion was upward at all levels (Fig. 18a).

The presence of the bright band in Fig. 16b indicates that cooling by melting was occurring in that layer, and most likely evaporation of raindrops was occurring to some degree below the melting layer. However, the amount of cooling by melting and evaporation was insufficient to produce a reversal of the net upward air motion in the lower troposphere in the stratiform region.

As a further indication that stratiform region downdrafts were relatively unimportant, the dropsondes obtained on the periphery of the stratiform region (Fig. 19) did not exhibit a signature of strong subsidence as seen in the vicinity of stratiform regions with mesoscale downdraft (i.e., Zipser's 1977 "onion sounding" was not evident). Both the Doppler radar and soundings thus indicate that the stratiform regions of the MCSs occurring in this tropical depression, at the time the depression was on the verge of tropical cyclogenesis, were
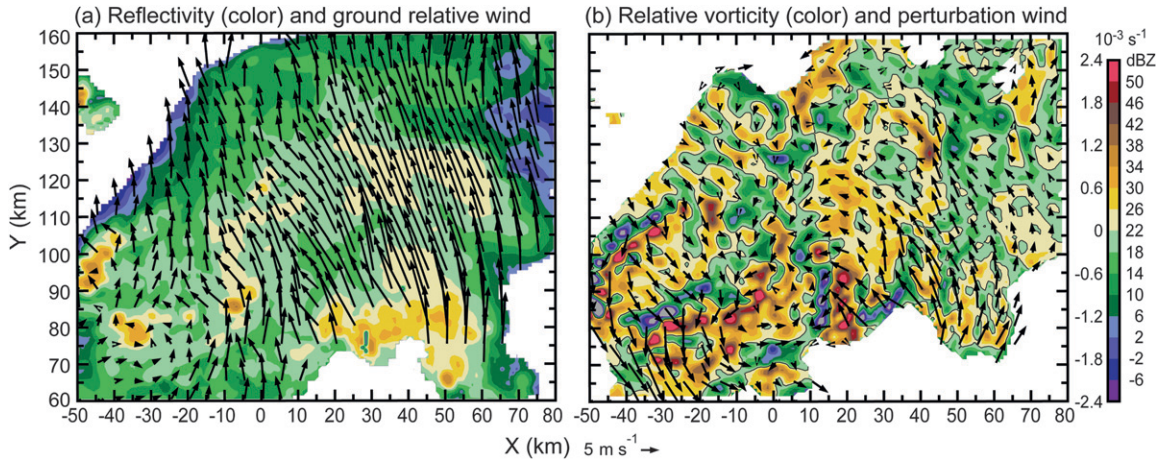
FIG. 17. ELDORA radar analysis of stratiform region at the 6-km level at 2005–2040 UTC. The domain is the same as in Fig. 16. (a) Reflectivity and earth-relative wind vectors. (b) Relative vertical vorticity (10^{-3} s^{-1}) and perturbation wind vectors. Note that the color scale in (b) is one order of magnitude smaller than that shown in Figs. 10–12, and vectors are scaled differently because of the larger domain size.

dominated by upward air motion and thus rather unlike the convection generally seen in ordinary MCSs.

6. Convective and stratiform contributions to cyclonic circulation

Figure 20 expresses the distribution of relative vorticity quantitatively. The black, green, and red curves in Fig. 20a show the average vorticity in the volumes sampled in the three fly-bys described previously in connection with Figs. 8a and 15. These three curves illustrate how the convective cells were concentrating vorticity at the lower levels in their earlier stages and then more in the midlevels at later times. Thus, the active convective cells created a positive vorticity perturbation at a sequence of levels, from the low to midlevels. These vorticity anomalies could then be axisymmetrized into the larger circulation of the depression.

In Fig. 20a, the blue curve is the profile of area-averaged vertical vorticity (ζ) shown by ELDORA in the stratiform region. It is small compared to the mean vorticity in the convective cell seen during the three ELDORA fly-bys (black, green, and red profiles in Fig. 20a). However, the area covered by the stratiform region is much larger than the area covered by the convective cell. To see the effect on the larger scale, we integrate the vorticity over area to obtain the circulation:

$$\Gamma \equiv \iint \zeta \, dA,$$

where A is the area. The circulation in the stratiform region at the 6-km level is shown by the blue bar in

Fig. 20b. The circulation at the times of the three fly-bys is shown by the black, green, and red bars in Fig. 20b. By the time of the third fly-by, the convective cell circulation is about 2/3 as large as the stratiform circulation, even though the stratiform region is more than 20 times larger in area than the convective cell (cf. the gray bars in Fig. 20b). As the stratiform region forms from the old, weakening convective cells, it accumulates the cyclonic rotation occurring in the upper reaches of the intense cell, as shown in Fig. 13. Since the cooling by melting and evaporation at and below the brightband level in the stratiform region were insufficient to produce net downward motion at the low levels (Fig. 18a), the net vertical mass transport in the stratiform region did not produce PV at the low levels as would be expected in an ordinary mesoscale convective system (Fritsch et al. 1994; Houze 2004). The vorticity occurring in the upper regions of the convective cells and accumulated in the stratiform region is available to be axisymmetrized into the larger circulation of the depression (Montgomery et al. 2006), thus, helping the depression intensify and ultimately become a tropical storm.

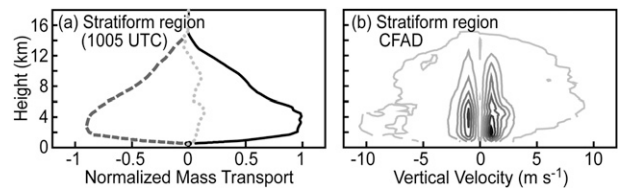As noted above, Zipser and Gautier (1978) also found that the intense convective feature in the intensifying

FIG. 18. As in Fig. 15, but for stratiform region in Figs. 16 and 17 and with contour intervals of 25×10^6 kg s^{-1}.
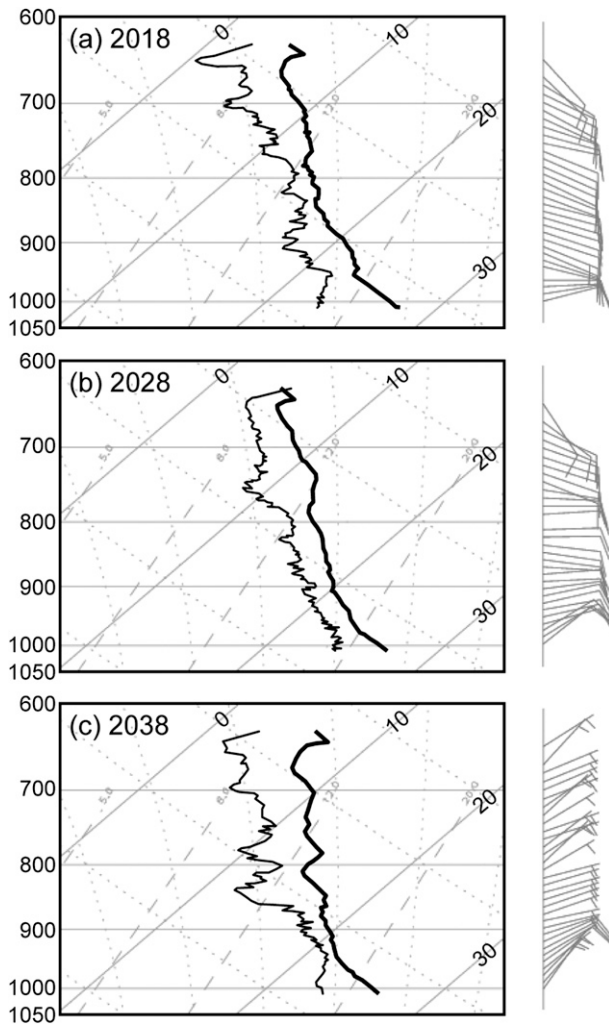
FIG. 19. Dropsonde data taken on the north side of the strati-form region. The locations of the soundings are in Fig. 7. Plots are in skew T–log p format. One wind barb = 10 m s^{-1}.
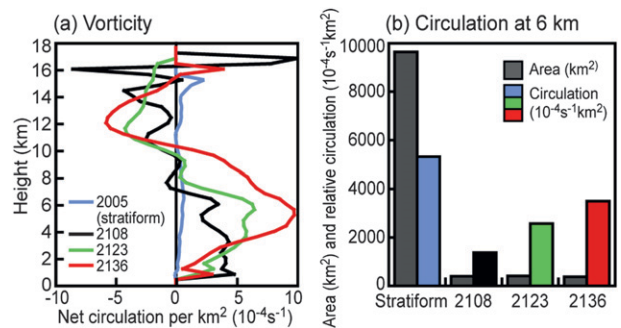

FIG. 20. (a) Average vorticity in the convective domains of Figs. 10–12 (black, green, and red) and the stratiform domain of Figs. 16 and 17 (blue). (b) Area and circulation in each domain.

vorticity downward since the convective cells generated PV at the lower levels, as shown by Fig. 14.

7. Conclusions

The ELDORA radar system aboard a RAINEX air-craft observed convection in the intensifying depression that became Hurricane Ophelia. One particular updraft was extensively sampled. The high-resolution wind field derived from the Doppler radar data showed that this updraft was *deep*—extending to a radar echo top of 17 km, *wide*—10 km in horizontal dimension, *strong*—with a vertical velocity of 10–25 m s^{-1} throughout the upper portion of the draft, and *vortical*—positive vorticity was concentrated within the updraft. Thermodynamic re-trieval performed on the Doppler wind field showed that the massive convective updraft had maximum buoyancy at about the 10-km level, likely boosted by latent heat of freezing. Although vortical convective updrafts in developing tropical depressions have been suggested in previous studies, this is the first direct ob-servational documentation of one. This updraft was part of an MCS, which had a stratiform precipitation region ~200 km in dimension. The updraft was similar in size and intensity to the wide, intense updraft described by Zipser and Gautier (1978) for an intensifying tropical depression off the coast of Africa. The present study verifies and extends their findings.

Zipser and Gautier (1978) estimated from low-level flight track wind data that the stretching of the low-level ambient vorticity by the mesoscale convergence feed-ing the massive convective updraft was sufficient to account for the intensification of the synoptic-scale de-pression vortex. The ELDORA data obtained in the depression examined in this study are consistent with this suggestion and further show the vertical distribution of mass flux through the depth of the convection. The vertical derivative of this mass flux is proportional to the

depression that they investigated was primarily an updraft feature. They noted that the downdrafts were weaker and comprised only a small vertical mass flux compared to the updraft. They further noted that in this respect the mesoscale convective entity differed from ordinary mesoscale convective systems, such as squall lines, which have extensive stratiform region downdrafts that play a role in the systems' dynamics.

It is doubtful that the weak downdrafts in the strati-form region of the MCS investigated here could have been substantially advecting vorticity downward, as would be necessary for a mechanism such as that of Bister and Emanuel (1997) to be effectual. We conclude that the stratiform region vorticity in this MCS pri-marily enhanced the depression's development at the midlevels. It was not necessary to advect this midlevel

vertical gradient of latent heating and thus is a proxy for the generation of positive PV by the giant convective cell. Figure 14b shows the concentration of the vertical gradient of vertical mass flux at low to midlevels within the updraft and its immediate surroundings.

The deep, wide, intense convective updraft of the MCS in the pre-Ophelia depression was generally unaided by downdraft dynamics—strikingly unlike the convective elements of more ordinary MCSs (Zipser 1977; Kingsmill and Houze 1999; Houze 2004). Although downdrafts occurred sporadically in the general region of convection within the depression, they did not dominate the vertical mass flux in the storm; rather, as suggested by Nolan's (2007) idealized simulations, the updraft mass transport dominated as the depression approached tropical storm stage. The detailed three-dimensional wind field associated with the mature giant intense convective cell sampled intensively by ELDORA showed no evidence of downdraft gust front convergence below the updraft. Thermodynamic retrieval indicated that evaporative cooling and precipitation drag occurred in the rain shower of the large cell, but were insufficient to produce a strong downdraft or gust front outflow to force the updraft. Zipser and Gautier (1978) also noted that evaporation cooled the air at low levels but there was no downward transport of lower equivalent potential temperature air into the boundary layer. They commented on how this lack of significant downdraft activity in an intensifying depression sets the observed convection apart from ordinary cumulonimbus.

Since downdraft gust front convergence was not occurring and forcing parcels to rise above their levels of free convection, some other dynamics must explain how the parcels originating in low levels became buoyant enough to produce such a massive updraft. The strong low-level winds of the depression were obtaining heat and moisture via boundary layer mixing enhanced by the low-level winds (Emanuel 1986, 1987; Yano and Emanuel 1991; Emanuel et al. 1994). In this respect, the depression was already behaving like a tropical cyclone, gaining energy from the sea surface rather than from the thermodynamic stratification of the environment. At this point in the storm's history, rather than supporting an eyewall, the wind-induced mixing was providing energy to support massive buoyant convective towers that were in turn carrying vorticity upward and distributing vorticity through the low to midlevels, thus preparing the depression for conversion to tropical cyclone dynamics.

The wind-induced mixing in the boundary layer produced air that had a steep lapse rate, little convective inhibition, and high equivalent potential temperature. When this rapidly flowing air encountered the rainy area of the giant cell, it converged with the low-level rain-cooled air at the base of the rain shower, rose easily above its level of free convection, and developed the extreme buoyancy and vertical acceleration seen in this study. Crook and Moncrieff (1988) showed in an idealized numerical modeling study that this form of lifting in response to a density gradient occurs where the low-level inflow air encounters the rain-cooled air of a convective system even if the cooled air is not spreading out as a density current. In this case the horizontal inflow does not stagnate at the cold pool boundary, but rising motion nonetheless occurs in connection with low-level convergence in the density gradient bounding the rain shower. They further found that this type of convective updraft forcing is particularly favored when the convection occurs in an environment of large-scale convergence and lifting. In this respect, the developing tropical cyclone would be an ideal environment for this type of non-gust-front convective triggering to occur.

The massive convective updraft investigated here was attached to a stratiform precipitation region, as is typical for an MCS (Houze 2004). However, on close inspection, this stratiform region exhibited some special characteristics. Most notably, the stratiform region was not dominated by downdraft motions at lower levels. The stratiform region likely formed from older, weakened convective cells, in the manner described by Houze (1997). The midlevel vorticity pattern in the stratiform region contained convective-scale vorticity anomalies, likely left behind by previously active convective cells, each of which likely had a cyclonic vorticity maximum collocated with the updraft, as in the cell analyzed in detail in this paper. Evidently the vortical motion contained in each convective updraft's upper portions was incorporated into the stratiform region, and over time gave the stratiform region a significant midlevel circulation. As such, the stratiform region of the MCS became a reservoir of positive vorticity generated in previously more active convective cells. At midlevels, the net circulation of the stratiform region exceeded that of the individual active convective cells.

Finally, we can speculate on how the positive vorticity stored in the massive convective cell and its associated stratiform region affected the cyclogenesis of Tropical Storm Ophelia a few hours after the aircraft mission described in this paper. As was shown in Fig. 5, the depression contained several MCSs of the general size and character of the one we have analyzed in detail, as well as some more isolated deep convective cells. In this respect, the developing depression consisted of a mix of convective cells and MCSs in various life cycle stages, as depicted conceptually in Fig. 1d. Each of the convective cells, during its intense active stage, whether separate or part of an MCS, generated PV in the low- to midtropospheric

layers of its massive updraft (as shown in Fig. 14b). As these intense updrafts weakened, some of the vorticity trapped within them was stored in a stratiform region in the form of an MCV. Thus, the MCSs embedded in the developing tropical cyclone contained both convective cells with convective-scale vorticity perturbations extending from the low to midlevels and stratiform regions with midlevel mesoscale vorticity perturbations. Since the stratiform region MCVs were derived from convective cells, both the active convective cells and the stratiform regions of MCSs embedded within the intensifying depression contained vorticity derived in a bottom-up process, in which convective cells generate the PV. The midlevel MCVs in stratiform regions might be enhanced by midlevel cooling by melting, but there is no necessity for the midlevel vorticity to extend downward since the convective cells generate vorticity through all the low to midlevels, as shown in Fig. 14.

Together the convective-scale perturbations at the lower levels and the mesoscale perturbations at the midlevels, all derived from the deep convective cells, contributed strongly to the total storm circulation. Montgomery et al. (2006) have shown via modeling how vorticity anomalies smaller in scale than the scale of the parent depression can be axisymmetrized into the mean flow to convert the depression into the structure of a tropical cyclone. We suspect that a process of this type, or approximately of this type, was responsible for the upscale transfer of vorticity from the convective and stratiform regions of MCSs like the one investigated here to the larger developing cyclone.

The data collected by ELDORA in the genesis stage of Ophelia during RAINEX thus present a picture of convection at this stage of tropical cyclone development that is extremely intense and concentrates positive PV throughout the lower half of the atmosphere via a combination of convective and mesoscale processes. The structure of the convection, with its absence of a downdraft gust front forcing the intense updraft and its overall similarity to the convection observed earlier by Zipser and Gautier (1978), demands further investigation by future field studies and/or high-resolution numerical modeling, to determine the full set of mechanisms by which this type of convection creates local PV anomalies to feed into and strengthen the parent vortex.

APPENDIX

Radar Analysis Methodology

The ELDORA data were initially corrected for navigation errors (Bosart et al. 2002) and manually edited using the NCAR Solo II software package (Oye et al. 1995) to remove noise, ocean returns, and radar artifacts. The edited reflectivities and Doppler velocities from the aft and fore radars were then interpolated to a 400-m Cartesian grid using an exponential distance-weighting function, with hydrometeor terminal fall speed contributions removed using empirical relationships from Joss and Waldvogel (1970) for rain and Atlas et al. (1973) for snow, following Marks and Houze (1987). These interpolated velocities were then synthesized using a variational approach described in detail in Reasor et al. (2009). This variational minimization matches the observed Doppler information to the gridded three-dimensional wind field while simultaneously enforcing the anelastic mass continuity equation, with vanishing second derivatives of the wind field and vertical velocity boundary conditions as weak constraints.

With the full wind and precipitation fields available, horizontal and vertical gradients of temperature and pressure perturbations can be deduced from the equations of motion and thermodynamic equation (Gal-Chen 1978; Houze 1993). The particular formulation used for this analysis follows the variational approach described by Roux and Ju (1990) and Roux et al. (1993). Perturbations were derived relative to a composite environmental sounding composed of nearby dropsondes and a radiosonde from Miami, Florida. A three-step Leise filter (Leise 1982) was applied prior to the retrieval, effectively limiting the resolved scales to a 3.2-km wavelength, with $V_0 = 1$ m s^{-1} and $W_0 = 0.5$ m s^{-1} threshold magnitudes of horizontal and vertical velocity, respectively, to prevent computational errors in some terms in the retrieval equations. Time derivatives were estimated using consecutive volumes. These were the data volumes for 2108 and 2123 UTC, illustrated in Figs. 8a,b, with an advective displacement correction of $U = -5.2$ m s^{-1} and $V = 2.2$ m s^{-1} determined by the

applied feature tracking. Centered time differencing was
used around the average of the two volumes (at 2108 and
2123 UTC) so the retrieval is valid for the approximate
median time (~2115 UTC). Relatively minor differences
were seen using a forward or backward time difference.
The retrieval yielded ''momentum-checking'' parame-
ters (Gal-Chen and Hane 1981) between 0.289–0.398,
indicating good internal consistency of the retrieval in the
absence of external validation.

REFERENCES

Aberson, S. D., M. L. Black, R. A. Black, R. W. Burpee, J. J. Cone, C. W. Landsea, and F. D. Marks Jr., 2006: Thirty years of tropical cyclone research with the NOAA P-3 aircraft. *Bull. Amer. Meteor. Soc.,* **87,** 1039–1055.

Atlas, D., K. R. Hardy, R. Wexler, and R. J. Boucher, 1963: On the origin of hurricane spiral bands. *Geofis. Int.,* **3,** 123–132.

——, R. C. Srivastava, and R. S. Sekhon, 1973: Doppler radar characteristics of precipitation at vertical incidence. *Rev. Geophys. Space Phys.,* **11,** 1–35.

Barnes, G. M., E. J. Zipser, D. Jorgensen, and F. D. Marks Jr., 1983: Mesoscale and convective structure of a hurricane rainband. *J. Atmos. Sci.,* **40,** 2125–2137.

Bister, M., and K. A. Emanuel, 1997: The genesis of Hurricane Guillermo: TEXMEX analysis and a modeling study. *Mon. Wea. Rev.,* **125,** 2662–2682.

Bosart, B. L., W.-C. Lee, and R. M. Wakimoto, 2002: Procedures to improve the accuracy of airborne Doppler radar data. *J. Atmos. Oceanic Technol.,* **19,** 322–339.

Bracken, W. E., and L. F. Bosart, 2000: The role of synoptic-scale flow during tropical cyclogenesis over the North Atlantic Ocean. *Mon. Wea. Rev.,* **128,** 353–376.

Bryan, G. H., and J. M. Fritsch, 2000: Moist absolute instability: The sixth static stability state. *Bull. Amer. Meteor. Soc.,* **81,** 1207–1230.

Crook, N. A., and M. W. Moncrieff, 1988: The effect of large-scale convergence on the generation and maintenance of deep moist convection. *J. Atmos. Sci.,* **45,** 3606–3624.

DeMaria, M., J. A. Knaff, and B. H. Connell, 2001: A tropical cyclone genesis parameter for the Atlantic. *Wea. Forecasting,* **16,** 219–233.

Emanuel, K. A., 1986: An air–sea interaction theory for tropical cyclones. Part I: Steady-state maintenance. *J. Atmos. Sci.,* **43,** 585–604.

——, 1987: An air–sea interaction model of intraseasonal oscillations in the tropics. *J. Atmos. Sci.,* **44,** 2324–2340.

——, J. D. Neelin, and C. S. Bretherton, 1994: On large-scale circulations in convecting atmospheres. *Quart. J. Roy. Meteor. Soc.,* **120,** 1111–1143.

Fritsch, J. M., J. D. Murphy, and J. S. Kain, 1994: Warm core vortex amplification over land. *J. Atmos. Sci.,* **51,** 1781–1806.

Gal-Chen, T., 1978: A method for the initialization of the anelastic equations: Implications for matching models with observations. *Mon. Wea. Rev.,* **106,** 587–606.

——, and C. E. Hane, 1981: Retrieving buoyancy and pressure fluctuations from Doppler radar observations: A status report. *Atmos. Technol.,* **13,** 98–104.

Gray, W. M., 1968: Global view of the origin of tropical disturbances and storms. *Mon. Wea. Rev.,* **96,** 669–700.

Halverson, J., and Coauthors, 2007: NASA's Tropical Cloud Systems and Processes (TCSP) Experiment: Investigating Tropical Cyclogenesis and Hurricane Intensity Change. *Bull. Amer. Meteor. Soc.,* **88,** 867–882.

Hence, D. A., and R. A. Houze Jr., 2008: Kinematic structure of convective-scale elements in the rainbands of Hurricanes Katrina and Rita (2005). *J. Geophys. Res.,* **113,** D15108, doi:10.1029/2007JD009429.

Hendricks, E. A., M. T. Montgomery, and C. A. Davis, 2004: On the role of ''vortical'' hot towers in formation of Tropical Cyclone Diana (1984). *J. Atmos. Sci.,* **61,** 1209–1232.

Heymsfield, G. M., J. B. Halverson, J. Simpson, L. Tian, and T. P. Bui, 2001: ER-2 Doppler radar investigations of the eyewall of Hurricane Bonnie during the Convection and Moisture Experiment-3. *J. Appl. Meteor.,* **40,** 1310–1330.

Hildebrand, P. H., and Coauthors, 1996: The ELDORA/ASTRAIA airborne Doppler weather radar: High-resolution observations from TOGA COARE. *Bull. Amer. Meteor. Soc.,* **77,** 213–232.

Houze, R. A., Jr., 1982: Cloud clusters and large-scale vertical motions in the tropics. *J. Meteor. Soc. Japan,* **60,** 396–410.

——, 1993: *Cloud Dynamics*. Academic Press, 573 pp.

——, 1997: Stratiform precipitation in regions of convection: A meteorological paradox? *Bull. Amer. Meteor. Soc.,* **78,** 2179–2196.

——, 2004: Mesoscale convective systems. *Rev. Geophys.,* **42,** RG4003, doi:10.1029/2004RG000150.

——, 2006: The Hurricane Rainband and Intensity Change Experiment: Observations and modeling of Hurricanes Katrina, Ophelia, and Rita. *Bull. Amer. Meteor. Soc.,* **87,** 1503–1521.

——, S. S. Chen, B. F. Smull, W.-C. Lee, and M. M. Bell, 2007: Hurricane intensity and eyewall replacement. *Science,* **315,** 1235–1239.

Joss, J., and A. Waldvogel, 1970: Raindrop size disribution and Doppler velocities. Preprints, *14th Conf. on Radar Meteorology,* Tucson, AZ, Amer. Meteor. Soc., 153–156.

Kingsmill, D. E., and R. A. Houze Jr., 1999: Kinematic characteristics of air flowing into and out of precipitating convection over the west Pacific warm pool: An airborne Doppler radar survey. *Quart. J. Roy. Meteor. Soc.,* **125,** 1165–1207.

Leise, J. A., 1982: A multi-dimensional scale-telescoped filter and data extension package. NOAA Tech. Memo. WPL-82, 19 pp.

Marks, F. D., Jr., and R. A. Houze Jr., 1987: Inner core structure of Hurricane Alicia from airborne Doppler radar observations. *J. Atmos. Sci.,* **44,** 1296–1317.

May, P. T., and D. K. Rajopadhyaya, 1999: Vertical velocity characteristics of deep convection over Darwin, Australia. *Mon. Wea. Rev.,* **127,** 1056–1071.

McTaggart-Cowan, R., G. D. Deane, L. F. Bosart, C. A. Davis, and T. J. Galarneau Jr., 2008: Climatology of tropical cyclogenesis in the North Atlantic (1948–2004). *Mon. Wea. Rev.,* **136,** 1284–1304.

Mechem, D. B., R. A. Houze Jr., and S. S. Chen, 2002: Layer inflow into precipitating convection over the western tropical Pacific. *Quart. J. Roy. Meteor. Soc.,* **128,** 1997–2030.

Montgomery, M. T., M. E. Nicholls, T. A. Cram, and A. B. Saunders, 2006: A vortical hot tower route to tropical cyclogenesis. *J. Atmos. Sci.,* **63,** 355–386.

Nolan, D. S., 2007: What is the trigger for tropical cyclogenesis? *Aust. Meteor. Mag.,* **56,** 241–266.

Oye, R., C. Mueller, and S. Smith, 1995: Software for radar translation, visualization, editing, and interpolation. Preprints, *27th Conf. on Radar Meteorology,* Vail, CO, Amer. Meteor. Soc., 359–363.

Reasor, P. D., M. T. Montgomery, and L. F. Boast, 2005: Mesoscale observations of the genesis of Hurricane Dolly (1996). *J. Atmos. Sci.,* **62,** 3151–3171.

——, M. D. Eastin, and J. F. Gamache, 2009: Rapidly intensifying Hurricane Guillermo (1997). Part I: Low-wavenumber structure and evolution. *Mon. Wea. Rev.,* **137,** 603–631.

Riehl, H., and J. S. Malkus, 1958: On the heat balance in the equatorial trough zone. *Geophysica,* **6,** 503–538.

Ritchie, E. A., and G. J. Holland, 1997: Scale interactions during the formation of Typhoon Irving. *Mon. Wea. Rev.,* **125,** 1377–1396.

——, J. Simpson, W. T. Liu, J. Halverson, C. Velden, K. F. Brueske, and H. Pierce, 2003: Present day satellite technology for hurricane research: A closer look at formation and intensification. *Hurricane! Coping With Disaster,* R. Simpson, Ed., Amer. Geophys. Union, 249–289.

Rotunno, R., 1981: On the evolution of thunderstorm rotation. *Mon. Wea. Rev.,* **109,** 171–180.

Roux, F., and S. Ju, 1990: Single-Doppler observations of a West African squall line on 27–28 May 1981 during COPT 81: Kinematics, thermodynamics, and water budget. *Mon. Wea. Rev.,* **118,** 1826–1854.

——, V. Marécal, and D. Hauser, 1993: The 12–13 January 1988 narrow cold-frontal rainband observed during MFDP/FRONTS 87. Part I: Kinematics and thermodynamics. *J. Atmos. Sci.,* **50,** 951–974.

Simpson, J., E. Ritchie, G. J. Holland, J. Halverson, and S. Stewart, 1997: Mesoscale interactions in tropical cyclone genesis. *Mon. Wea. Rev.,* **125,** 2643–2661.

Sippel, J. A., J. W. Nielsen-Gammon, and S. E. Allen, 2006: The multiple vortex nature of tropical cyclogenesis. *Mon. Wea. Rev.,* **134,** 1796–1814.

Steranka, J., E. B. Rodgers, and R. C. Gentry, 1986: The relationship between satellite measured convective bursts and tropical cyclone intensification. *Mon. Wea. Rev.,* **114,** 1539–1546.

Willoughby, H. E., 1988: The dynamics of the tropical hurricane core. *Aust. Meteor. Mag.,* **36,** 183–191.

——, F. D. Marks Jr., and R. J. Feinberg, 1984: Stationary and moving convective bands in hurricanes. *J. Atmos. Sci.,* **41,** 3189–3211.

Xu, K.-M., and K. A. Emanuel, 1989: Is the tropical atmosphere conditionally unstable? *Mon. Wea. Rev.,* **117,** 1471–1479.

Yano, J.-I., and K. A. Emanuel, 1991: An improved WISHE model of the equatorial atmosphere and its coupling with the stratosphere. *J. Atmos. Sci.,* **48,** 377–389.

Yuter, S. E., and R. A. Houze Jr., 1995a: Three-dimensional kinematic and microphysical evolution of Florida cumulonimbus. Part II: Frequency distribution of vertical velocity, reflectivity, and differential reflectivity. *Mon. Wea. Rev.,* **123,** 1941–1963.

——, and ——, 1995b: Three-dimensional kinematic and microphysical evolution of Florida cumulonimbus. Part III: Vertical mass transport, mass divergence, and synthesis. *Mon. Wea. Rev.,* **123,** 1964–1983.

——, and ——, 1997: Measurements of raindrop size distributions over the Pacific warm pool and implications for *Z–R* relations. *J. Appl. Meteor.,* **36,** 847–867.

Zipser, E. J., 1977: Mesoscale and convective-scale downdrafts as distinct components of squall-line circulation. *Mon. Wea. Rev.,* **105,** 1568–1589.

——, 2003: Some views on "hot towers" after 50 years of tropical field programs and two years of TRMM data. *Cloud Systems, Hurricanes, and the Tropical Rainfall Measuring Mission (TRMM): A Tribute to Dr. Joanne Simpson, Meteor. Monogr.,* No. 51, Amer. Meteor. Soc., 49–58.

——, and C. Gautier, 1978: Mesoscale events within a GATE tropical depression. *Mon. Wea. Rev.,* **106,** 789–805.

——, D. J. Cecil, C. Liu, S. W. Nesbitt, and D. P. Yorty, 2006: Where are the most intense thunderstorms on earth? *Bull. Amer. Meteor. Soc.,* **87,** 1057–1071.